

EXPERIMENTAL CHARACTERISATION OF IMAGE LINE DISCONTINUITIES AND REALISATION OF BAND PASS FILTER

A Thesis Submitted

in Partial Fulfillment of the Requirements

for the Degree of

Master of Technology

by

MAJOR P. K. CHOUDHARY

to the

DEPARTMENT OF ELECTRICAL ENGINEERING
INDIAN INSTITUTE OF TECHNOLOGY, KANPUR

29 Jan 1997

12 MAR 1997

CENTRAL LIBRARY
I. I. T. KANPUR

Acc. No. A-123207

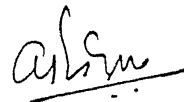
EE-1997-M-CMO-EXP



CERTIFICATE

This is to certify that the work contained in the thesis entitled EXPERIMENTAL CHARACTERISATION OF IMAGE LINE DISCONTINUITY AND REALISATION OF BAND PASS FILTER by MAJOR P. K. CHOUDHARY has been carried out under my supervision and that this work has not been submitted elsewhere for a degree.

Date: 29/1/97



Dr. ANIMESH BISWAS

Assistant Professor,

Department of Electrical Engineering,

Indian Institute of Technology, Kanpur

Abstract

Image line is a type of transmission line which is widely used as a transmission medium in microwave and millimetric wave regions Two types of discontinuities in this type of line viz. air gap and notch have been experimentally characterized as a T-network lumped element circuit using Transverse resonance technique. The line has been assumed as lossless and phase constant β_z has been experimentally obtained Subsequently, a band pass filter based on air gap discontinuity reactance parameters has been designed which was found to work experimentally very close to its designed parameters.

Acknowledgements

At the outset I shall place a deep sense of gratitude and appreciation to my thesis supervisor Dr. Animesh Biswas who visualised the concept of the presented work. He not only guided the academic work with a tremendous insight of subject, which he possesses in abundance, but also constantly encouraged me at times which used to get very much loaded with a sense of frustration. Many a number of hours spent in microwave lab bear testimony of theoretical and experimental accumen which he could introduce in measurement procedures.

I am also indebted to Dr. M. Sachidanand who introduced us to some of the basic tenets of microwave passive and active circuit design. A special word of thanks are due to Dr. Utpal Das, who always gave valuable advice whenever I approached him.

I shall be failing from my duty, if I do not acknowledge help rendered to me in academics and social fields by my friends Pawan, J. Kumar, and Ashish Patni. I am sure all three of them will establish themselves as pioneers in field of Microwave research in future. I am also grateful to Mrs. Rajeev Shukla, and Apu Sivas and for guiding me out and discussing concept used in project work. Thanks are due to Maj. R. K. Sharma for debugging the software problems encountered in otherwise a purely experimental project.

I shall place my deep sense of appreciation to Mr. V. K. Shrivastava of Central Workshop, who provided invaluable help in terms of repeated machining of dielectric material. Also, I shall thank all my fellow colleagues who helped me out of problems in writing this report.

I am extremely grateful to my parents Dr. J. N. Choudhary and Mrs. Pratima Choudhary, whose inspiration and upbringing could bring me to the portals of my present achievements. I am also indebted to my wife Komal and my little son Vaibhav for silently bearing the burdens of my idiosyncracies.

Last but not the least I am amused at vicissitudes of destiny which fills human life with both dark and bright colors with admirable dexterity.

Contents

1	INTRODUCTION	1
1.1	IMAGE GUIDE A PREVIEW	1
1.2	FIELD DISTRIBUTIONS IN IMAGE LINE	2
1.3	REASONS FOR UNDERTAKING PRESENT WORK	4
1.4	SCOPE AND ORGANISATION OF THESIS	5
2	TRANSVERSE RESONANCE TECHNIQUE,BASIS FOR EXPERIMENTAL SET-UP AND FINDING OUT PHASE CONSTANT	9
2.1	RESONANCE FREQUENCY METHOD	9
2.2	TRANSVERSE RESONANCE METHOD	10
2.3	EXPERIMENTAL SET-UP	12
2.3.1	SELECTION OF DIELECTRIC MATERIAL	14
2.3.2	ASPECT RATIO	18
2.3.3	MEASUREMENT ORGANISATION	19
2.4	APPROACH ADOPTED FOR THE EXPERIMENT	21
2.5	DETERMINATION OF PHASE CONSTANT β	22
3	CHARACTERISATION OF AIR-GAP TYPE OF DISCONTINUITY	28
3.1	A SAMPLE CALCULATION	28
3.2	ELEMENTARY EXPLANATION OF NORMALISED REACTANCE VALUES RESULTS	30
4	CHARACTERISATION OF NOTCH TYPE OF DISCONTINUITY	42
4.1	A SAMPLE CALCULATION	43
4.2	COMPARISON OF SCATTERING PARAMETERS AND REACTANCE VALUES OF T-NETWORK MODEL FOR AIR-GAP AND NOTCH TYPE OF DISCONTINUITY	44

5	REALISATION OF A BAND PASS FILTER USING AIR GAP DISCONTINUITY IN IMAGE LINE	60
5.1	SPECIFICATIONS OF THE FILTER	60
6	CONCLUSION	68
6.1	RECOMMENDATIONS	69
	References	70
	BIBLIOGRAPHY	71

List of Figures

1.1	VARIOUS CONFIGURATIONS OF IMAGE LINE	3
1.2	THE CROSS SECTION OF DIELECTRIC IMAGE LINE	6
1.3	FREQUENCY Vs PHASE CONSTANT(NORMALISED)	7
1.4	8
2.1	IMAGE LINE CAVITY (a)CROSS-SECTIONAL VIEW (b)LONGITUDINAL VIEW	13
2.2	EQUIVALENT CIRCUIT REPRESENTATION OF IMAGE LINE CAVITY	14
2.3	T-NETWORK REPRESENTATION OF DISCONTINUITY	15
2.4	EVEN AND ODD MODE ANALYSIS OF T-NETWORK MODEL	16
2.5	A LOSSLESS LINE (a)WITHOUT DISCONTINUITY (b)WITH DISCONTINUITY	17
2.6	(a)Cut-off frequencies for 1st higher order mode(b)Dispersion bandwidth against different aspect ratio and dielectric constant	24
2.7	(a)Schematic diagram of experiment set-up (b) Dielectric line (c)Air-gap discontinuity (d)Notch discontinuity	25
2.8	PHASE CONSTANT WITH VARYING LATERAL WALLS OF HOUSING	26
2.9	COMPARISION OF THEORETICAL AND EXPERIMENTAL PHASE CONSTANT	27
3.1	S21 MAGNITUDE PARAMETER OF AIR GAP TYPE OF DISCONTINUITY FROM 8.146 - 9.243 GHz	31
3.2	S21 MAGNITUDE PARAMETER OF AIR GAP TYPE OF DISCONTINUITY FROM 9.59 - 11.19 GHz	32
3.3	S21 MAGNITUDE PARAMETER OF AIR GAP TYPE OF DISCONTINUITY FROM 11.68 -12.1 GHz	33

3.4	S21 PHASE PARAMETER FOR AIR GAP FROM 8.146-11.19 GHz ..34
3.5	S21 PHASE PARAMETER FOR AIR GAP FROM 11.68-12.10 GHz ..35
3.6	AIR GAP REACTANCE AGAINST GAP LENGTH FROM 8.146-9.59 GHz ..38
3.7	AIR GAP REACTANCE AGAINST GAP LENGTH FROM 10.42-12.1 GHz...39
3.8	AIR GAP REACTANCE Vs FREQUENCY FOR 1cm AND 1.5cm GAP LENG'
3.9	AIR GAP REACTANCE Vs FREQUENCY FOR 2cm AND 2.5cm GAP LENG'
4.1	S21(MAGNITUDE) FOR NOTCH FROM 8.146-9.243 GHz.....47
4.2	S21(MAGNITUDE) FOR NOTCH FROM 9.590-11.19 GHz.....47
4.3	S21(MAGNITUDE) FOR NOTCH FROM 11 68-12.1 GHz48
4.4	S21(PHASE) FOR NOTCH FROM 8.146-11.19 GHz.....49
4.5	S21(PHASE) FOR NOTCH FROM 11 68-12.1 GHz..50
4.6	REACTANCE(SERIES) FOR NOTCH FROM 8.146-8.697 GHz.....51
4.7	REACTANCE(SERIES) FOR NOTCH FROM 9.243-11.19 GHz 52
4 8	REACTANCE(SERIES) FOR2NOTCH FROM 11.19-12.1 GHz.....53
4.9	REACTANCE(SHUNT) FOR NOTCH FROM 8.146-9.59 GHz.....54
4.10	REACTANCE(SHUNT) FOR NOTCH FROM 10.42-12.10GHz.....55
4.11	REACTANCE(SERIES) FOR NOTCH Vs FREQUENCY.....56
4.12	REACTANCE(SHUNT) FOR NOTCH Vs FREQUENCY at WIDTH 0.5 cm..57
4.13	REACTANCE(SHUNT) FOR NOTCH Vs FREQUENCY at WIDTH 1.0 cm..58
4.14	REACTANCE(SHUNT) FOR NOTCH Vs FREQUENCY at WIDTH 2.0,2.5 cm
5.1	GUIDE WAVELENGTH Vs FREQUENCY.....64

5.2	K Vs AIR GAP LENGTH.....	65
5.3	PHI Vs AIR GAP LENGTH	66
5.4	A SCHEMETIC DIAGRAM OF BAND PASS FILTER.....	67
5 5	S21 Vs FREQUENCY FOR BAND PASS FILTER.....	67

List of Tables

2.1	PROPERTIES OF SOME IMPORTANT DIELECTRIC MATERIALS . . .	18
2.2	COMPARISON OF THEORETICAL AND EXPERIMENTAL PHASE CONSTANT	23
3.1	NORMALISED SERIES REACTANCE VALUES OF EQUIVALENT T- NETWORK MODEL OF AIR GAP DISCONTINUITY	37
3.2	NORMALISED SHUNT REACTANCE VALUES OF EQUIVALENT T- NETWORK MODEL OF AIR GAP DISCONTINUITY	37
4.1	NORMALISED SERIES REACTANCE VALUES OF EQUIVALENT T- NETWORK MODEL OF NOTCH TYPE DISCONTINUITY	46
4.2	NORMALISED SHUNT REACTANCE VALUES OF EQUIVALENT T- NETWORK MODEL OF NOTCH TYPE DISCONTINUITY	46
5.1	VARIATION OF K AND ϕ WITH DISCONTINUITY WIDTH	62

Chapter 1

INTRODUCTION

Considerable advances have been made in recent past in the field of Information Technology(IT) Many new types of value- added services are being provided to customers throughout the globe.It has,in turn,added new demands on various different types of transmission media which carry information bearing signals used to provide such services Continuous research is being pursued to upgrade the utility and application of existing transmission facilities in upper microwave and sub-millimetric wave region(.5mm to 5mm wavelenght) It is not only the transmission, but also the utility of transmission lines in fabrication of active and passive microwave components which attract much attention of researchers Dielectric Image line is one of such novel transmission lines which lends itself to very practical and cost effective circuit technique. In upper-Microwave and sub millimetric wave regions Waveguides,Planar and quasi-planar transmission lines like Microstrip and finlines suffer a disadvantage of very high loss and smaller dimensions The component fabrication ,as a consequence,becomes a problem It is in such a situation that alternatives like Image line can become very useful.

1.1 IMAGE GUIDE:A PREVIEW

The configuration of a Image line and its variations are shown in fig 1.1.It comprises of a rectangular dielectric slab of relative permittivity (ϵ_r) backed by a perfectly conducting ground plane.It was first proposed by Marcatali[1] and Goel[2].The image line supports hybrid modes like EH_{mn} and HE_{mn} [ref section 1.2 for mode designation]. The presence of ground plane resolves the degeneracy,because the strongest elementary field component of E_{11}^x mode that would have been existing at the center of dielectric

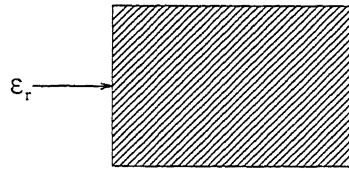
guide gets shorted out and single mode operations over a considerable frequency range is possible. The ground plane also provides a heat sink and is very convenient for dc biasing of active devices for integrated circuits. In higher frequency ranges, transmission line sections made of dielectric guide has larger dimensions than those fabricated from other conventional lines and it makes fabrication of oscillators, mixers, phase shifters filters from such lines relatively easier. Low dielectric constant materials ($\epsilon_r = 2-3$) are generally selected as these are less dispersive and thus provide wide band of operations.

1.2 FIELD DISTRIBUTIONS IN IMAGE LINE

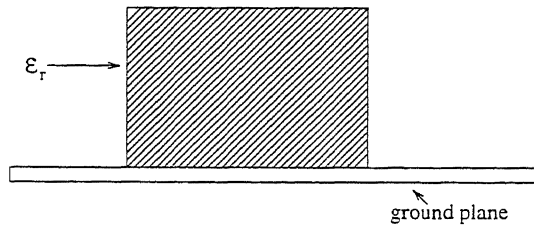
The possible designation of modes in a Image line is E(TM) having only E_z, E_y and H_x components and H(TE) having only H_z, H_y and E_x components. [Direction of axes are referred as in fig 1.2] In this way the mode of dielectric Image line is designated as EH if the field strenghts E_z, E_y and H_x are superior to the field strenghts H_z, H_y and E_x . Similarly the mode is called HE if the contrary is true.

For increased confinement of fields inside the dielectric material and to minimise the losses due to radiation and conduction plane some other variations of image line have been suggested in the literature which has been shown in fig 1.1. Several methods are available for analysing image guide and to find out its propagation characteristics. Klaus Solbach and Ingo Wolff carried out a detailed study of higher order propagating modes of dielectric image line by using hybrid mode analysis based on mode matching technique [3]. The investigated structure of Solbach and Wolff has been shown in fig 1.2. It comprises of two coupled image lines of width '2w' and heighth 'h' separated by a distance 'c'. The structure is enclosed between a bottom and a top ground planes. The properties of a single uncoupled line has been calculated by taking $b = c/2 = \text{infinity}$. The entire field region has been subdivided into four partial regions and a complete set of field solutions has been obtained for each sub area. The important results have been shown in fig 1.3 and in fig 1.4. In fig 1.3 phase constant of single image line normalised to ($k_0 = \omega\sqrt{\epsilon_0\mu_0}$) is shown for three lowest order modes. It shows that fundamental mode is EH_{11} mode which has no cutoff frequency. Phase constants of higher modes exist only for frequencies higher than a cutoff frequency.

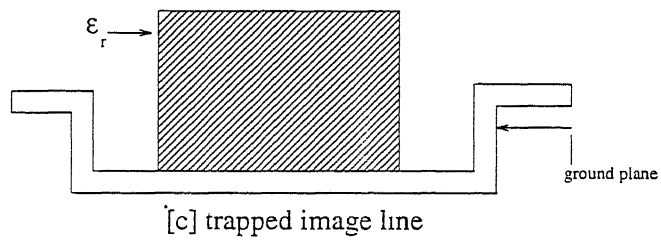
In fig 1.4 the magnetic and electric field distributions of the EH_{11} fundamental mode on a single dielectric image line are shown. Fig 1.4(a) is applicable for lower frequencies whereas fig 1.4(b) is valid for higher frequencies. It is clear from both the figures that a



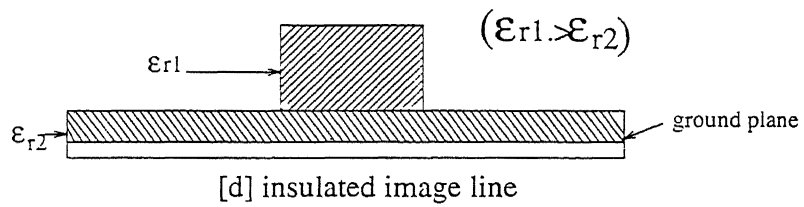
[a] rectangular dielectric guide



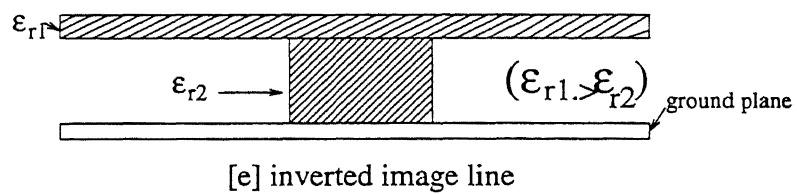
[b] image guide



[c] trapped image line



[d] insulated image line



[e] inverted image line

Figure 1.1: VARIOUS CONFIGURATIONS OF IMAGE LINE

very prominent difference exists in the field decay outside the dielectric. As the frequency is increased from a lower to a higher value, more and more energy gets concentrated inside the dielectric material.

In fig 1.4(c) the field distribution of a image line of larger width has been shown. A greater amount of electromagnetic energy gets concentrated inside the dielectric material when width of dielectric is more. Also it is fairly clear from above figures 1.3 to 1.4 that fundamental EH_{11} mode is very nearly transverse magnetic(TM).

1.3 REASONS FOR UNDERTAKING PRESENT WORK

Most of the Microwave circuits invariably employ sections of uniform transmission structures as basic building block. However, these sections are generally accompanied by discontinuity of some type or other e.g. step change in dimension, air gap, bends etc. Since most of the times these discontinuities are unintentional, efforts are made to reduce them as far as possible. But at the same time there are certain discontinuities which are purposefully introduced to make use of reactance associated with them to achieve certain circuit function viz. an iris in a coaxial line, inductive or capacitive post in a waveguide, gap in central conductor of a stripline etc.

For a comprehensive understanding of design of a microwave circuit it is essential that the discontinuities, which may crop up or are intended to be introduced, are characterised completely. Since the discontinuity dimension is generally much smaller than the wavelength, it is usually represented by a lumped element circuit. When the longitudinal dimension of discontinuity is very short, the equivalent circuit consists of a single shunt or series connected reactance located at the point of discontinuity. However, when the discontinuity has a larger longitudinal extent, the equivalent circuit is generally a π or a T- network.

An accurate characterization of discontinuity is regarded as more essential for microwave integrated circuit. It is because of the fact that microstrip circuits, especially in monolithic configuration do not lend themselves to adjustment or tuning after the fabrication of circuit is complete. If provision is made for later adjustments, the main advantage of compactness and reproducibility of MICs is partially lost. Hence, microstrip, stripline and finline discontinuities have been studied extensively in recent years. However, not much literature is available on discontinuity analysis in image lines. Since image line holds

a promising future as a popular type of transmission medium in microwave and millimetric wave region, discontinuity analysis in such a line was deemed to be a productive exercise.

Also, a band pass filter based on image line discontinuity parameters offers certain advantages as compared to conventional waveguide filters. In waveguide filters, machining and positioning of posts and irises is a very critical task. Any irregularity in machining, particularly at the points where such elements join waveguide walls, gives large inaccuracies in results. On the other hand, filters designed by the method undertaken in present work gives a very simple and uncomplicated fabrication procedure. Since an image line comprises of only a dielectric rod placed over a ground plane, the filter designed will be a lightweight and compact structure, in which only fabrication involvement will be pasting the dielectric pieces over any ground plane. It will have an additional benefit of cheap cost of production. The filter thus produced envisages to be of much use in most of the applications, particularly keeping in the mind that by selecting a dielectric material of high dielectric constant (ϵ_r), filters of very sharp quality factor (Q) can be realised. Above all, the approach adopted in present work is slated to be a novel method of realising a filter.

1.4 SCOPE AND ORGANISATION OF THESIS

This thesis is devoted to experimental characterisation of two types of image line discontinuities such as air gap and notch. Propagation phase constant β_z has also been ascertained experimentally. Subsequently, a band pass filter based on reactance parameters of air gap discontinuity has been designed and its experimental result has been presented.

In chapter 2 the design concept employed in experimental set-up has been explained. The basis of experimental organisation is Transverse resonance technique, presented by Itoh and Sorrentino [4] which has been modified for analysis of finline structures by Animesh Biswas [5]. The theoretical enumeration of this technique precedes design considerations used for carrying out the experiment. The method employed for measuring propagation constant of investigated image line along with the results also find place in this chapter. These results have been compared with theoretical results obtained by Pradhan [6]. Before the results were extracted the software developed in [6] was suitably modified and integrated as a package for this purpose. In chapter 3 the experimental results along with rudimentary theoretical explanations for T-network modelling of a air

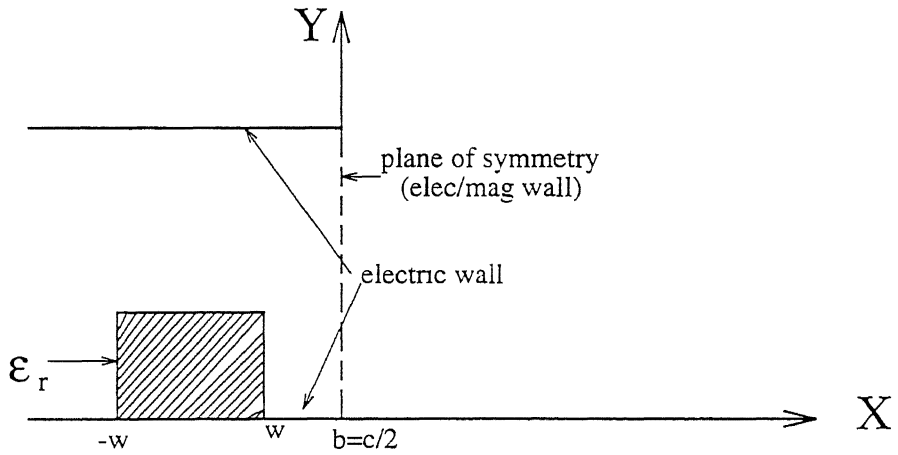
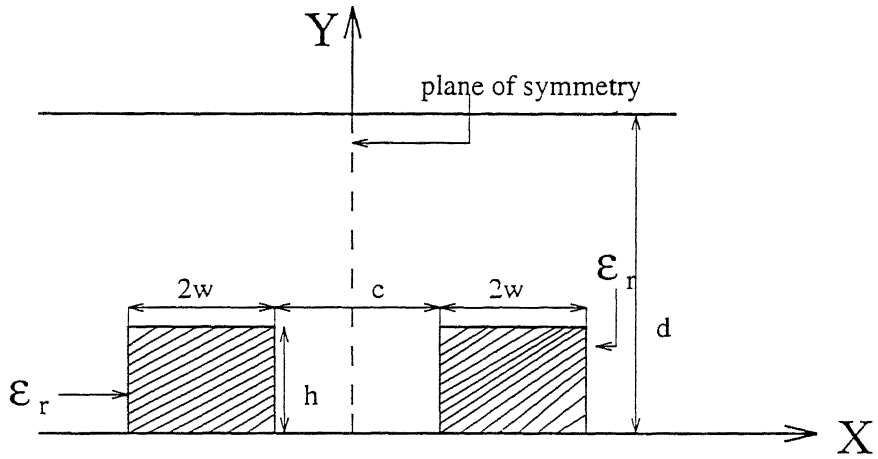


Figure 1.2: THE CROSS SECTION OF DIELECTRIC IMAGE LINE

gap discontinuity in a shielded image line has been presented. In chapter 4 the application of the same theory for the notch type of discontinuity and its results has been presented. A comparison of experimental results obtained in analysis of both air gap and notch discontinuity has also been presented in this chapter. In chapter 5 a detailed band pass filter design based on air gap discontinuity accompanied by experimental results has been submitted.

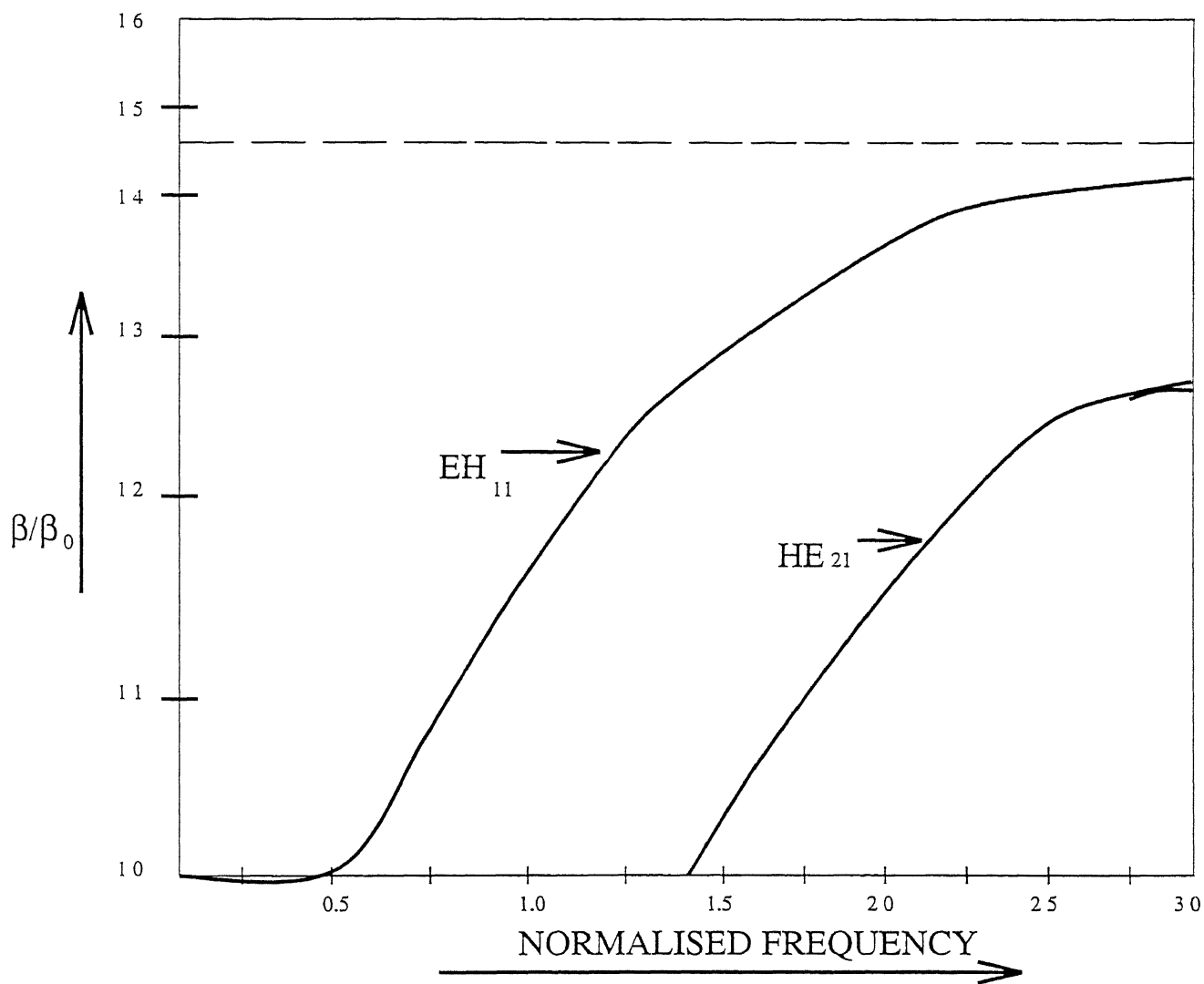


Figure 1.3: FREQUENCY Vs PHASE CONSTANT(NORMALISED)

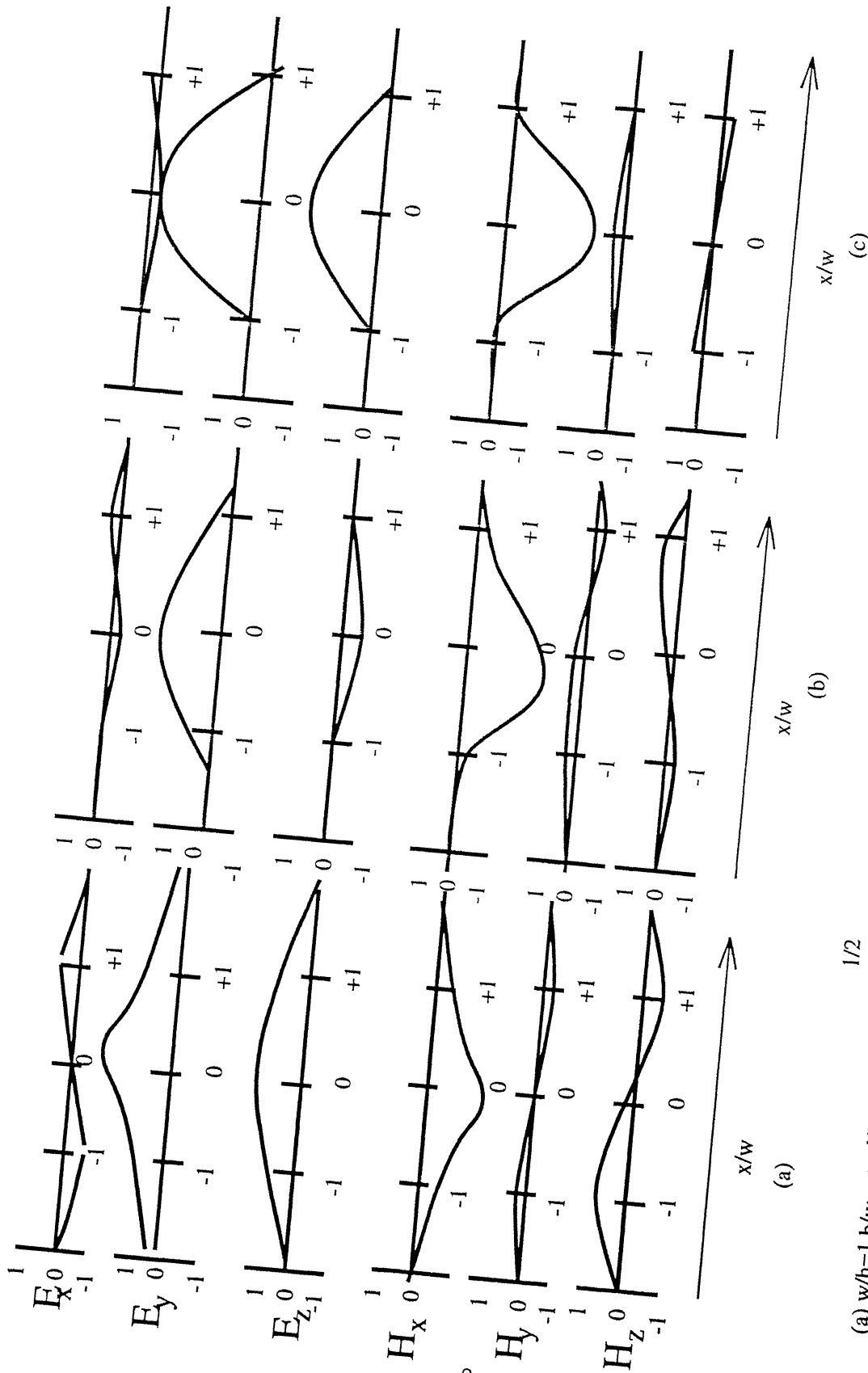


Figure 1.4:

(a) $w/h=1, b/w=\alpha, d/h=a, B=4\ln(\epsilon_r-1)/c=1.2, \beta/\beta_0=1.854$ (b) $B=3.0, \beta/\beta_0=1.42$ (c) $B=1.25, \beta/\beta_0=1.3183$

NORMALISED FIELD DISTRIBUTION OF THE EH_{1/2} ON A DIELECTRIC IMAGE LINE

Chapter 2

TRANSVERSE RESONANCE TECHNIQUE, BASIS FOR EXPERIMENTAL SET-UP AND FINDING OUT PHASE CONSTANT

Many innovative experimental methods have been used from time to time to characterise transmission line discontinuities. Some of these methods have been enumerated in succeeding paragraphs.

2.1 RESONANCE FREQUENCY METHOD

Pic and Hoefer[7] devised an experimental method to characterise step and symmetric inductive strip discontinuity in finlines. The method consists of finding the resonance frequency of a cavity containing a section of finline with the discontinuity. Resonance frequency of the cavity was measured at two different positions of discontinuity, one at the center and other at one quarter wavelength away from the center and then the resonance condition is applied. However, the accuracy of equivalent circuit parameters of discontinuity is highly dependent upon exactness of experimental process.

2.2 TRANSVERSE RESONANCE METHOD

This technique was first used by Sorrentino and Itoh [4] to find out equivalent circuit parameters of step, strip and notch types of discontinuity in a bilateral finline. The transverse resonance condition of a resonator is equivalent to setting the total admittance at any plane of the resonator cavity equal to zero. The condition of resonance can be theoretically found out by satisfying the boundary condition of the fields at each interface of the cavity and subsequently making use of orthogonal properties to get a homogeneous system of equations. The resonant frequency of the cavity of a fixed length in the presence of discontinuity can be determined by setting the coefficient matrix of homogeneous equations equal to zero. The application of transverse resonance condition at the discontinuity junction will provide the equivalent circuit parameters. It has been, however, assumed that higher order modes generated by the discontinuity will not reach the cavity walls.

By setting total reactance at any plane in the cavity equal to zero, the impedance parameters of any discontinuity inside the cavity can be determined. Fig 2.1 shows the cross-section and longitudinal view of image line cavity with an arbitrary discontinuity and fig 2.2 shows its equivalent circuit representation. If a symmetrical discontinuity is placed symmetrically inside the image line cavity, the resonance condition in terms of T-network parameters can be found out.

Let us consider the discontinuity as a T-network whose series and shunt reactances normalised with respect to characteristic impedance of image line are $\overline{x_{se}}$ and $\overline{x_{sh}}$ respectively [fig 2.3a]. In fig 2.3b the same T-network has been shown with $\overline{x_{sh}}$ split in two identical parts of values $\frac{\overline{x_{sh}}}{2}$ each joined in parallel. Also being a symmetrical structure the analysis can be done only for half of the circuit by considering both odd and even modes of excitation. Let l_e and l_m be the resonant length of image line connected to the T-network for odd and even modes respectively and β be the phase constant of the same line.

Now applying the transverse resonance condition at both sides of plane T_1 we have [ref fig 2.4a],

$$Y_{in1} + Y_{in2} = 0 \quad (2.1)$$

In odd mode of excitation, the reactance $\overline{x_{sh}}$ gets shorted out due to short circuit placed at the termination. Hence, we have [ref fig 2.4b],

$$\overline{x_{se}} + j \tan \beta l_e = 0 \quad (2.2)$$

$$s_{21}^T = e^{-j2\theta} \frac{(\tan\beta l_e - \tan\beta l_m)}{(1 - j\tan\beta l_e)(1 - j\tan\beta l_m)} \quad (2.9)$$

Expressing tangent terms in way of sine and cosine, we get,

$$s_{21}^T = j \frac{e^{-j2\theta} \left[\frac{\sin\beta(l_e - l_m)}{\cos\beta l_e \cos\beta l_m} \right]}{\left[\frac{(\cos\beta l_e - j\sin\beta l_e)(\cos\beta l_m - j\sin\beta l_m)}{\cos\beta l_e \cos\beta l_m} \right]} \quad (2.10)$$

After cancelling out identical terms from the above equation and writing exponential expression for sin and cosine expression, we are left with simple expression as follows

$$j \sin\beta(l_e - l_m) \frac{e^{-j2\theta}}{[e^{-j\beta l_e} e^{-j\beta l_m}]} \quad (2.11)$$

This is same as,

$$j \sin\beta(l_e - l_m) e^{j\beta(l_e - l_m) - 2\theta} \quad (2.12)$$

Expressing θ in terms of length 'l' and gap length '2s' we get the following expression:-

$$S_{21}^T = j \sin[\beta(l_e - l_m)] e^{j\beta(l_e + l_m - L + 2s)} \quad (2.13)$$

This is the expression of S_{21} as measured on the plane of termination of connecting transmission line since equation 2.5 is ABCD parameters of T-network as seen at the plane of discontinuity itself. As mentioned earlier, equation 2.7 has $e^{-j2\theta}$ term since ABCD parameters as obtained in equation 2.5 has been converted to S parameter and then shifted for phase by length L. Now if we set $\beta l = 0$ in equation 2.13 we get transmission S parameter of the discontinuity only

$$s_{21}^D = j \sin[\beta(l_e - l_m)] e^{j\beta(l_e + l_m + 2s)} \quad (2.14)$$

The important point to note here is that above expression gives S parameter of discontinuity only but as measured at the plane of termination of connecting transmission line.

2.3 EXPERIMENTAL SET-UP

The important design considerations for experimental set-up were as follows:-

- Selection of dielectric material

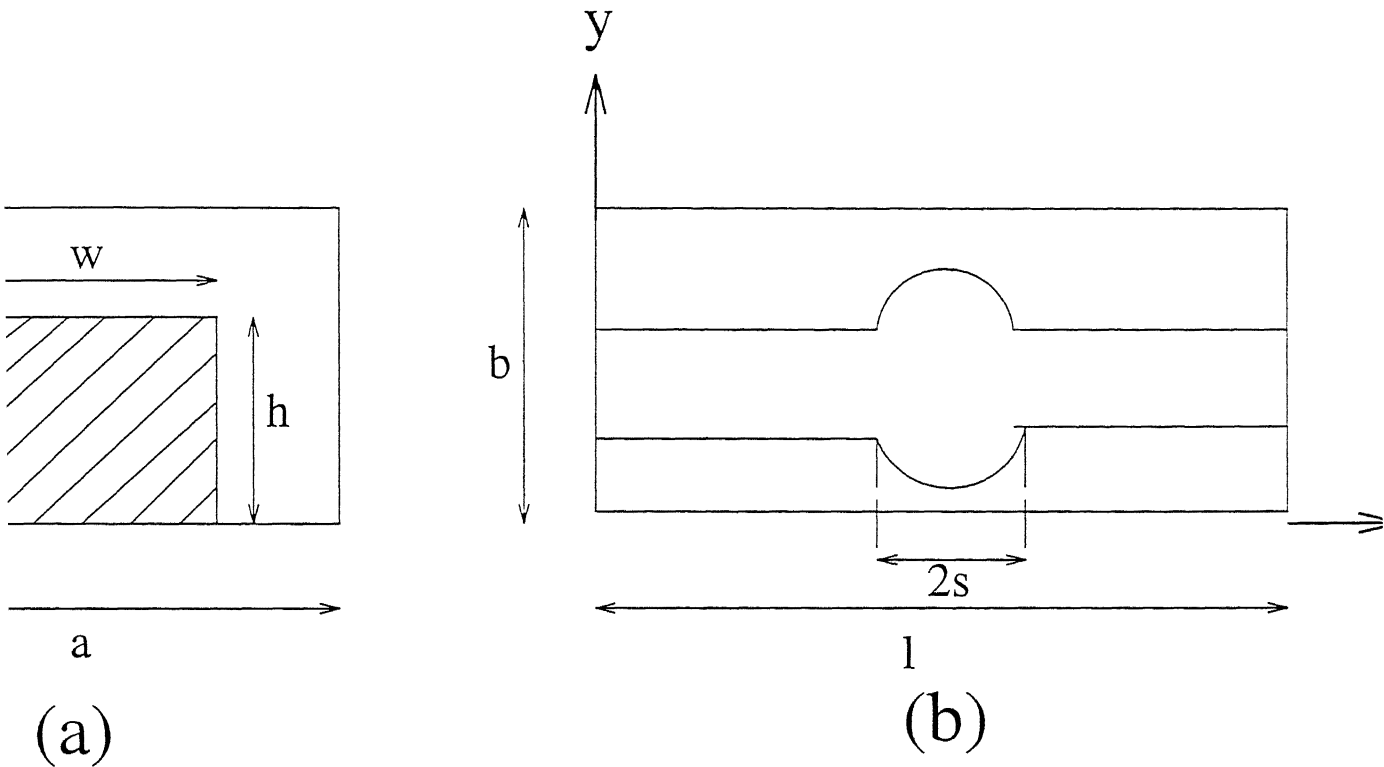


Figure 2.1. IMAGE LINE CAVITY (a)CROSS-SECTIONAL VIEW (b)LONGITUDINAL VIEW

- Dimensions(aspect ratio) of dielectric material
- Method of launching energy and measurement

Each one of the above was to be carefully decided for convenience of carrying out measurement as well as to take adequate care of some of the important Electromagnetic considerations which should be opti mised to the maximum These considerations were as follows.-

- Low dispersion
- Good wave-guiding property
- Low radiation loss

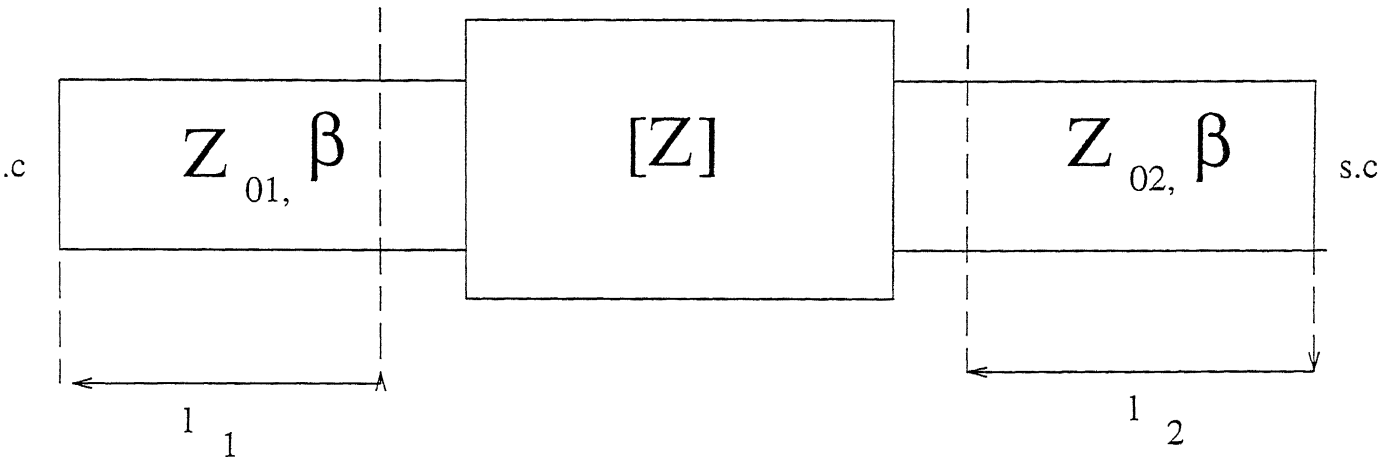


Figure 2.2. EQUIVALENT CIRCUIT REPRESENTATION OF IMAGE LINE CAVITY

2.3.1 SELECTION OF DIELECTRIC MATERIAL

Selection of dielectric material is an important step of designing experimental set-up since in image lines, unlike waveguides, dielectrics are used to guide energy rather than the metal wall structures. In region of wavelength from 5 mm to optical wavelength a metal wall structure will cause attenuation due to skin effect. These skin effect losses denoted by α_c , are proportional to the square root of frequency. In the case of dielectric losses (denoted by α_d), these losses are due to the shunt conductance of the dielectric and depends upon resistivity or polarisation and dimensions of the dielectric material. At higher frequencies these losses can be made much less than conduction losses.

The important properties of the required dielectric material are listed below:-

- Should be easily machinable
- Should have low temperature sensitivity and high melting point
- Should provide decided bandwidth of operations
- Should be easily available

Table 2.1 gives important properties of several frequently used dielectric materials. Klaus Solbach[8] has given experimental results for image lines fabricated out of Parafin wax and stycast resins. Both are thermoplastic and parafin wax, because of its low melting point (50 degree celsius), though, very suitable for mass production by die-casting process, was ruled out for this experiment due to its temperature sensitivity and low mechanical strength which makes it difficult to machine. Similarly Stycast resin, which,

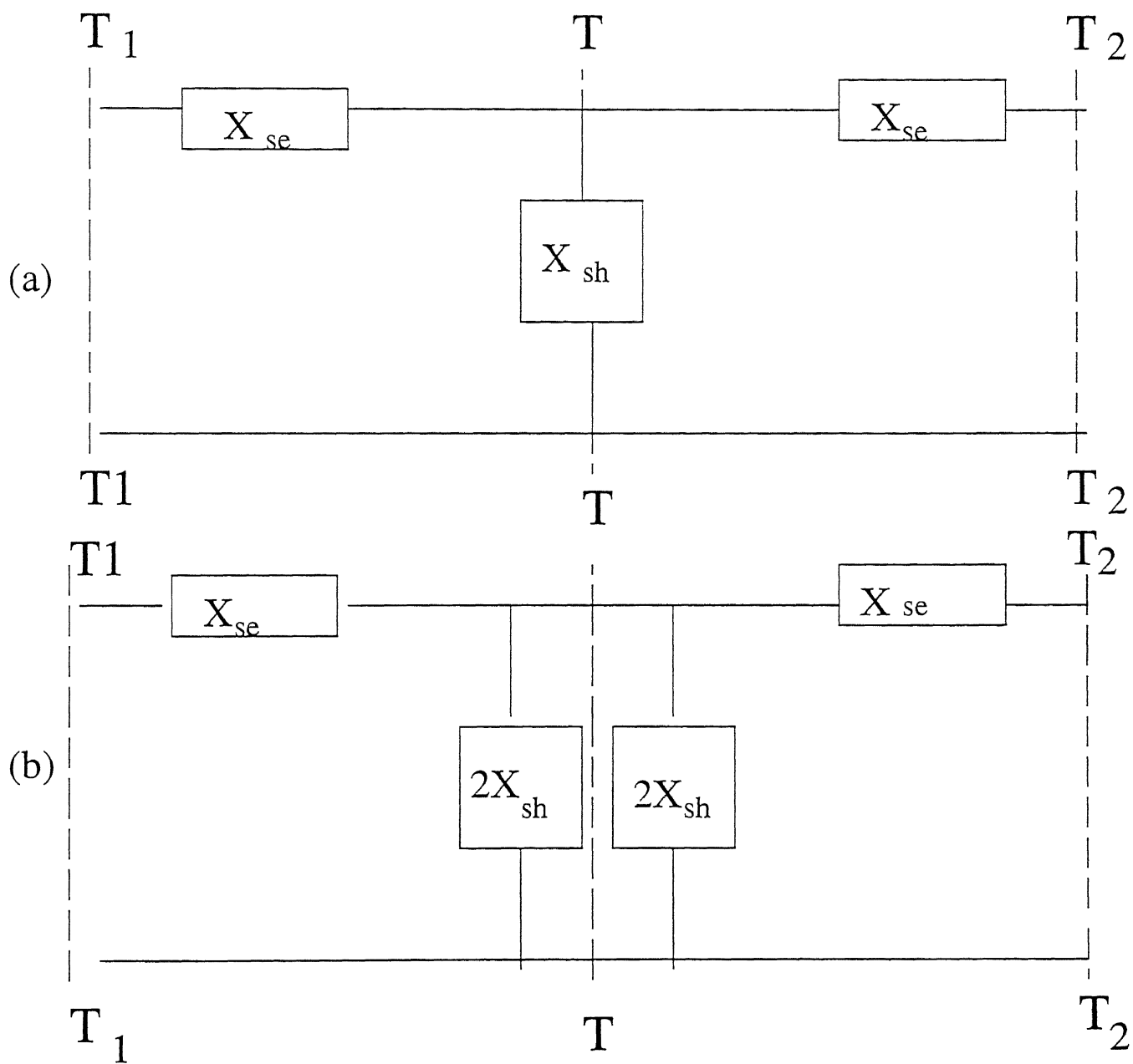


Figure 2.3: T-NETWORK REPRESENTATION OF DISCONTINUITY

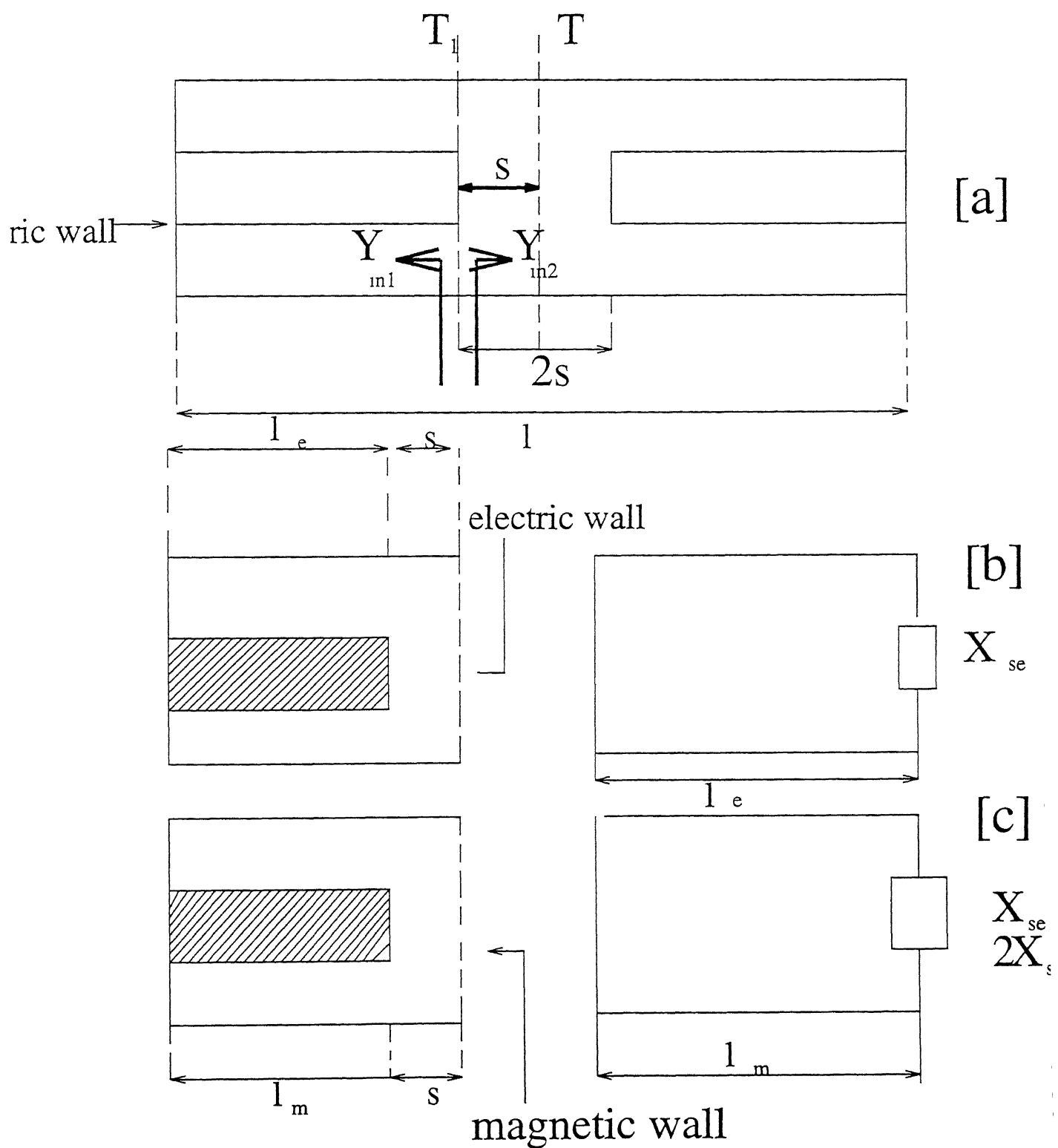


Figure 2.4: EVEN AND ODD MODE ANALYSIS OF T-NETWORK MODEL

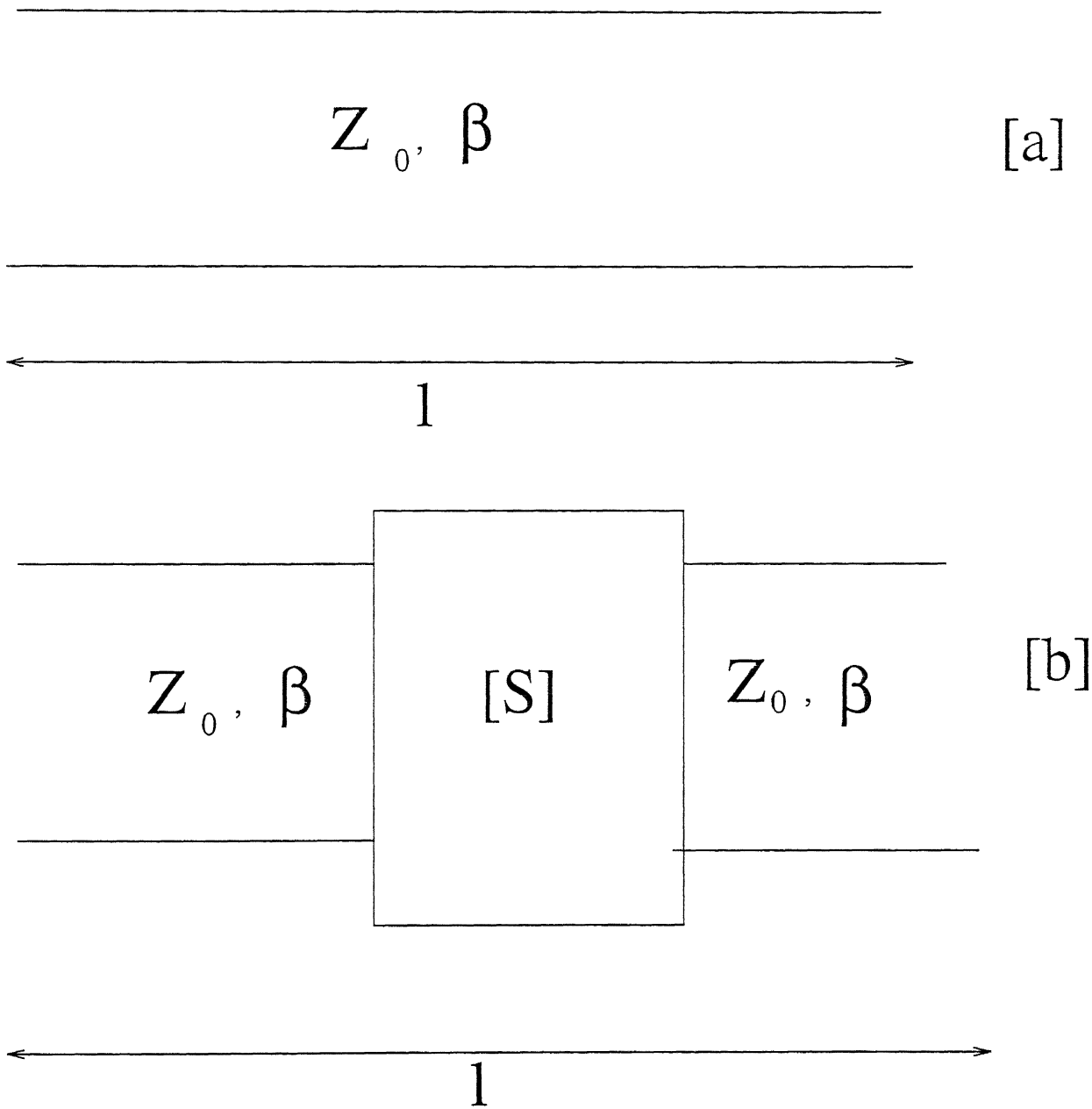


Figure 2.5: A LOSSLESS LINE (a)WITHOUT DISCONTINUITY (b)WITH DISCONTINUITY

	Teflon	RT/Duroid5880	Fused quartz	Parafin wax	Resin
Dielectric constant	2.1	2.2	3.78	2.22	3.4
Loss Tangent	.0005	.001	.0001	.0006	.0002
Machinability	good	good	very poor	poor	poor

Table 2.1: PROPERTIES OF SOME IMPORTANT DIELECTRIC MATERIALS

cross links to Polysterene at moderate temperatures,requires to be cured for 12 hours before it can be used and, thus is not highly sutable for experimental purposes as this set-up envisaged. There are other resins offering a range of dielectric constants from 3-25, such as 3M's High-k 707 ,but these are not easily available

If the material has a small dielectric constant it will be a disadvantage if high Q circuits are to be produced. But it is ,at the same time, an advantage if fundamental field distribution of any transmission line are to be examined since a better part of electromagnetic field is outside dielectric medium ,than in the air The loss tangent of stycast material is higher as compared to the others and having lower Q it is unsuitable for resonators or filters of smaller bandwidth.

Collier and Birch[9] have examined various parameters involved in deciding bandwidth of image guide viz. dielectric constant and aspect ratio. Fig 2.6(a) gives cut-off frequency of first higher order mode for different aspect ratio and dielectric constant. It is evident that lower dielectric constant gives better bandwidth performance. Fig 2.6(b) shows dispersion bandwidth (which gives lower cut-off frequency) against aspect ratio and dielectric constant. Again it is seen that for a particular aspect ratio lower dielectric constants give greater bandwidth. However, if we consider good waveguiding property (lesser energy travelling in air compared to that in image guide) we find that higher dielectric constants are more suitable (ref fig 1.4). Collier and Birch[9] have calculated an optimum value of dielectric constant from these two contrasting requirements and an ideal value of $\epsilon_r = 2.5$ has been recommended.

It was decided to select Teflon ($\epsilon_r = 2.1$) for experiment since besides being very near to suggested dielectric constant of 2.5 it satisfied other requirements of easy machining and convenient procurement.

2.3.2 ASPECT RATIO

If we see fig 1.4(c) ,we find that far better confinement of electromagnetic fields result in an image line on a guide of higher thickness. Both Collier and Birch[9] and Klaus

Solbach [10] have suggested unity aspect ratio ($w/h = 1$) with investigated dimension being $2w/h$ for an experimental set-up of Image line. The reason for such an aspect ratio is that at these dimensions first two higher order modes E_{12}^x and E_{21}^x are degenerate. When the experimental measurements were taken for small thickness of Teflon material keeping the aspect ratio as 1, no substantial observations could be made on network analyser. Subsequently, as suggested by Collier and Birch [9] and Solbach [10] it was decided to take aspect ratio as $2w/h$ and dimensions selected based on preliminary observations of experiment were as follows:-

- $2w = 1.8$ cm
- $h = 0.9$ cm
- length $l = 15.4$ cm

2.3.3 MEASUREMENT ORGANISATION

Apart from selection of the dielectric material and its dimensions other major components of experimental set-up were:-

- Method of launching energy
- Prevention of radiation losses
- Tool for probing fields on the guide

■ *METHOD OF LAUNCHING ENERGY*

Several techniques have been employed to conduct measurements on dielectric image line in centimeter and millimetric wave regions. King and Schesinger [11-13] utilised metal waveguide mode launchers to launch and decouple the waves on dielectric image lines. The measurement of the wave amplitude on the dielectric line was made on the metal waveguide part of the measuring set-up. Itoh [14] also used the same method to find out field distribution of inverted strip dielectric waveguide. Klaus Solbach [15] has described electric measurement of image line in 26 - 90 GHz freq range. He, also, has used a rectangular metal waveguide type of mode launcher. Among the various other methods adopted by other authors is a vertical slot in the ground plane to be used as a mode launcher [10].

It was decided to adopt the method suggested by Solbach[15], since it was compatible with the rectangular metal X-band waveguide housing for the image line(as will be discussed later) as well as for the ease of fabrication.Fig 2.7 describes the schematic diagram of experimental set-up.It shows X-band metal waveguide type of adopters used as mode launcher It is suggested to fill the portion of adopter above the image guide surface with some absorbing material in order to minimise the reflections on the line.Fig 2.7 also shows tapered edges at both ends of image guide.It was done for smooth change over of fields from X-band mode launcher to surface of image line so that reflections on the line are minimum The same mechanism has been adopted by Solbach[15] to reduce VSWR to a minimum in his experimental set-up Initially for the air gap type of discontinuity analysis a 10 mm slant of taper was used,but,as will be seen in some of the plots of chapter 3, it resulted in some amount of standing wave on the line.Accordingly,the slant of the taper was increased upto 20mm in subsequent measurements of notch discontinuity and filter synthesis and reflections were reduced appreciably.

■ *REDUCTION OF RADIATION LOSSES*

To reduce the large amount of radiations of energy from the image guide surface, placing it inside a metallic waveguide type of housing has been suggested by Solbach[16] and Robert M.Knox[17].Another approach suggested to circumvent radiation losses was to use periodic structure in radiation free stopband mode as tuning and matching devices or to use Yagi-Uda antenna array as mode launcher[18].Solbach and Wolff[3] have studied the field parameters of a image line with a top conducting wall placed at some variable finite distance.

Pradhan[6] has done the study of propagation characteristics of a shielded image line with a upper as well as a lateral wall.The software developed for this work was modified for the dimensions of X-band rectangular waveguide type of shielding and theoretical impact of the same on propagation parameters was observed.The results have been submitted in Fig 2.8.It will be observed that effect of dispersion increases as upper and side walls are brought closer to the line.Here,keeping the upper wall at a constant height of a X-band dimension of 10.16 mm the lateral walls have been brought nearer to the dielectric line.Observations for side wall distance of 200 mm,40 mm and 11.43 mm(X-band waveguide broader side dimension) have been shown against normalised frequency (all frequencies are normalised by a factor as $B = freq * \frac{4h\sqrt{\epsilon_r-1}}{c_0}$ where c_0

is the velocity of light in vacuum) It is evident that lowering of side wall distance does not have much impact on frequencies in 8 – 12GHz region Since reduction in lateral wall distance have major impact on lower cut-off frequency only and considering the fact that the fundamental mode has zero cut-off in a image line and our experiment was to be conducted for higher frequency range, it was considered safe to enclose the image line in a waveguide type of housing and launch energy through a compatible X-band rectangular waveguide adapter. In addition, it was thought at the conceptual stage of designing the set-up that such an arrangement would facilitate guide wavelength measurement for phase constant β_z determination by slotted waveguide method where the line under investigation is kept inside a similar waveguide.

■ HOW TO PROBE THE FIELD

Solbach[15] has given the design of an electric probe using a miniature 50 ohms coaxial cable with partially removed outer conductor and soldered at a distance of quarter wavelength away from the ends of a $RG - (90/U)$ or $RG - (96/U)$ metal waveguide. It was, in turn, soldered to another metal waveguide tunable detector and complete probe was mounted on a three axis vernier mechanism. Since the present investigation envisaged use of a slotted waveguide for field measurement, it was decided not to fabricate this complicated probe structure. However, later on, slotted waveguide technique gave problems as with the optimum dimensions of the dielectric line, the pin of the coaxial detector started scratching the surface of the image line. Subsequently, an altogether different approach was used to find out β_z by means of phase measurements of scattering parameters on a network analyser HP 8410.

2.4 APPROACH ADOPTED FOR THE EXPERIMENT

In accordance with transverse resonance theory and experimental set-up enumerated earlier in section 2.1 following approach was adopted for carrying out the investigations:-

1. Using the experimental set-up described above i.e. a dielectric image line of Teflon material of width=18 mm, height=9 mm and length=154 mm with tapered edges on both ends of 10/20 mm slant, enclosed in a X-band rectangular metal waveguide housing with energy launched from a compatible X-band adapter, we have found

out transmission scattering parameter (S_{21}) of air gap and notch discontinuity by a Network Analyser HP 8410. Semi-rigid coaxial cable was used for connecting the Network Analyser with image line and a oscillator of type Wavetek model freq range 7.4-12.5 GHz was used as a source

2. For precise frequency measurements a frequency counter HP was connected to Network Analyser through a 20 dB down direction coupler.
3. The scattering parameters were also measured on Network Analyser HP 8510 at IIT DELHI.
4. Using equations 2.2 and 2.3 we have found out series and shunt normalised reactance parameters of equivalent T-Network model $\overline{X_{se}}$ and $\overline{X_{sh}}$ of the discontinuities respectively.
5. Using the measured air-gap discontinuity parameters, we have designed and tested a Band Pass Filter

2.5 DETERMINATION OF PHASE CONSTANT

β

Harold Jacobs et al [19] have given a technique of finding the guide wavelength λ_g in rectangular dielectric waveguide using a Gunn diode imbedded in rectangular dielectric cavity. This was done to examine the feasibility of using dielectric with minimum metal structure as a resonant cavity for working as an oscillator. Due to complex fabrication procedure involved, a different approach was followed which is enumerated in succeeding paragraphs.

The experimental procedure involved finding the total phase change in two different image line with same cross-sectional dimension but having lengths l_1 and l_2 . Two different waveguides housings of lengths similar to corresponding image lines were also fabricated. Length l_e is the effective length of the dielectric line which protrudes outside the housing inside the mode launcher. A Network analyser HP 8410 was used to carry out the experiment. Let β be the phase constant of an empty waveguide and β_1 be the phase constants of similar structures having image line of length l_1 . The experimental procedure adopted is as follows:-

Ser.No.	Freq in GHz	β_0 rad/mm	$\beta(\text{theory})$ rad/mm	β (measured) rad/mm	$\beta/\beta_0(\text{theory})$	$\beta/\beta_0(\text{expt})$
1	8.146	0.1706	.1715	.1815	1.005	1.06
2	8.697	0.1821	.192	.2021	1.054	1.09
3	9.243	0.1935	.21	.213	1.085	1.10
4	9.59	0.2008	.239	.2409	1.19	1.20
5	10.42	0.2182	.258	.2683	1.182	1.23
6	11.19	0.2343	.288	.2905	1.23	1.244
7	11.68	0.2446	0.249	.253	1.018	1.03
8	12.10	.2534	.26	.263	1.02	1.04

Table 2.2 COMPARISION OF THEORETICAL AND EXPERIMENTAL PHASE CONSTANT

- The empty waveguide for length l_1 of image line was connected to the Network Analyser and phase reading corresponding to it was made as zero for reference.
- Then the image line for this housing was inserted inside and phase reading for transmission coefficient was noted. Let this be θ_1 .
- The same above two steps were repeated for the image line of length l_2 Let this time the phase reading be θ_2

Now, we have,

$$\beta_1(l_1 + 2l_e) - \beta l_1 = \theta_1 \quad (2.15)$$

$$\beta_1(l_2 + 2l_e) - \beta l_2 = \theta_2 \quad (2.16)$$

Solving above two equations, we get,

$$\beta_1 = \frac{\theta_1 - \theta_2}{l_2 - l_1} + \beta \quad (2.17)$$

The tabular representation of measured ' β ' values has been given in table 2.2. A comparison of measured β values with those generated from Pradhan[6] has been given in fig 2.9. It shows the similarity between the nature of two results and highlights the zero cut-off for the fundamental mode and rise of second higher order mode at around 11.5 GHzs.

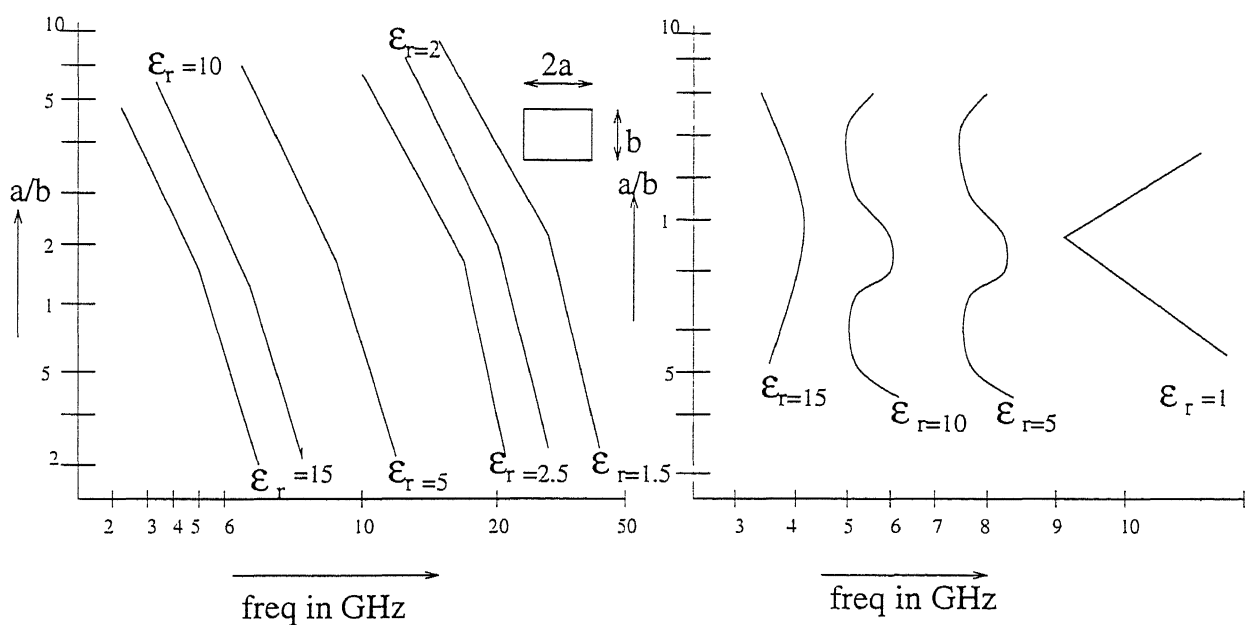


Figure 2.6. (a) Cut-off frequencies for 1st higher order mode (b) Dispersion bandwidth against different aspect ratio and dielectric constant

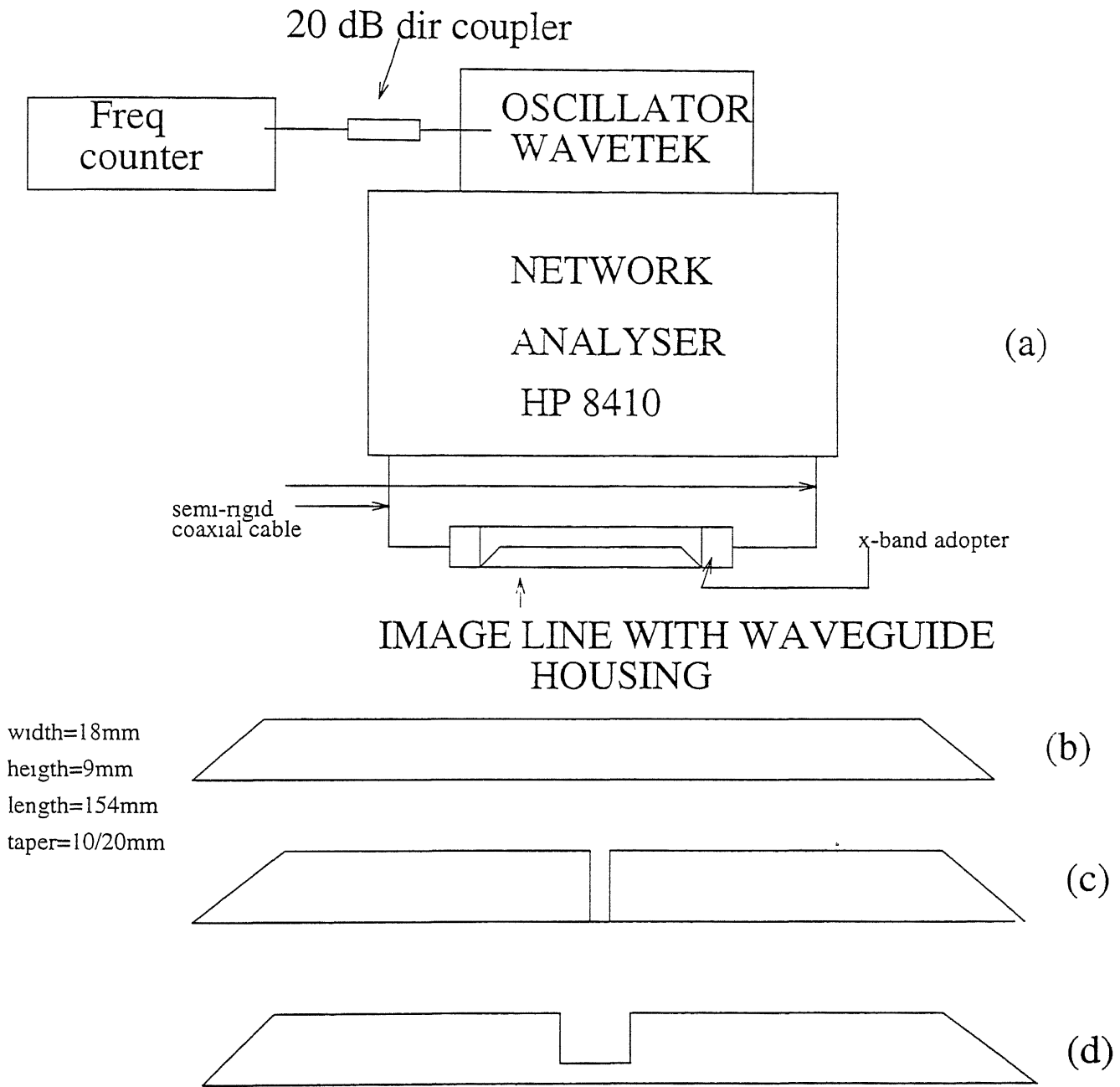


Figure 2.7: (a) Schematic diagram of experiment set-up (b) Dielectric line (c) Air-gap discontinuity (d) Notch discontinuity

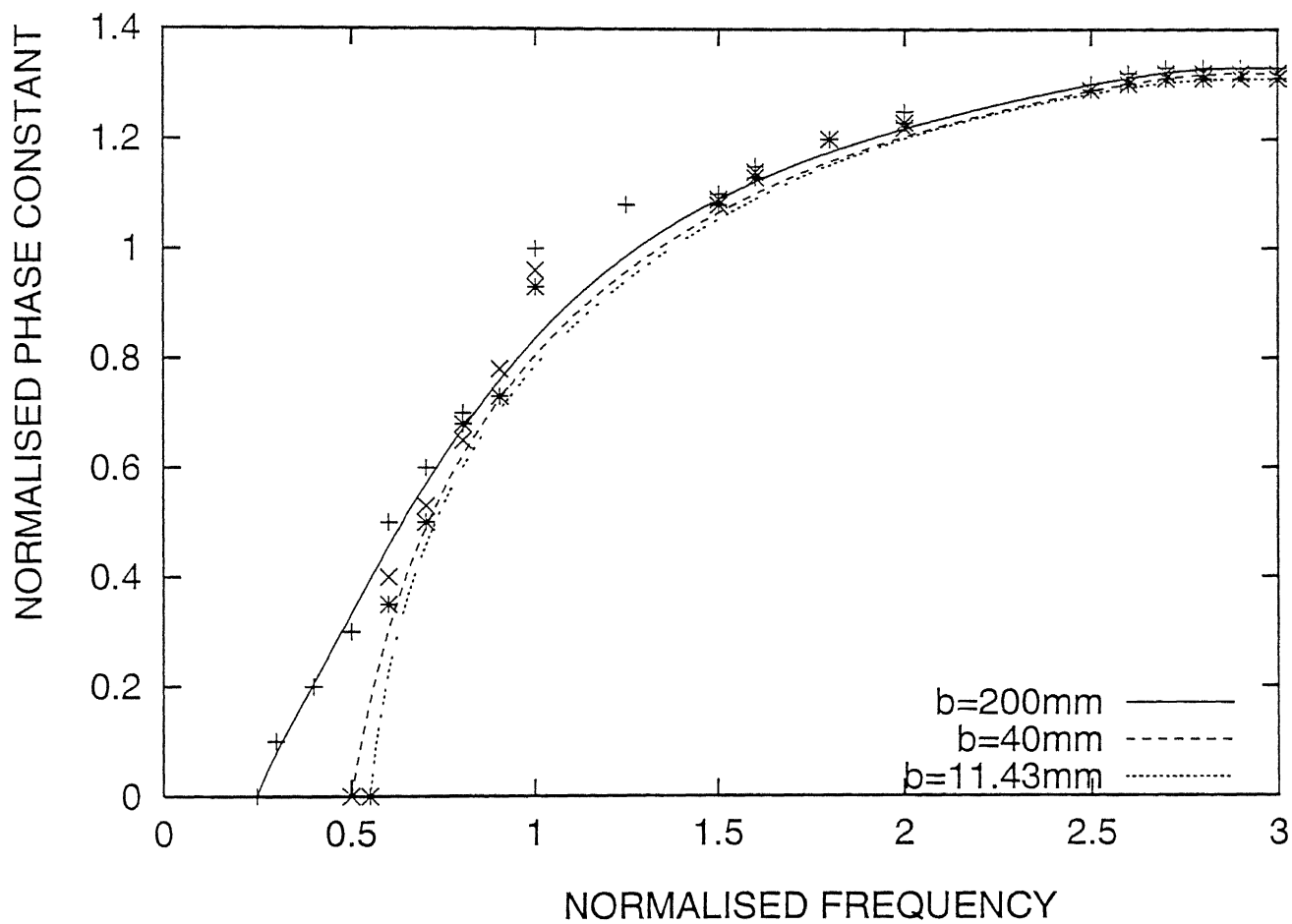


Figure 2.8: PHASE CONSTANT WITH VARYING LATERAL WALLS OF HOUSING

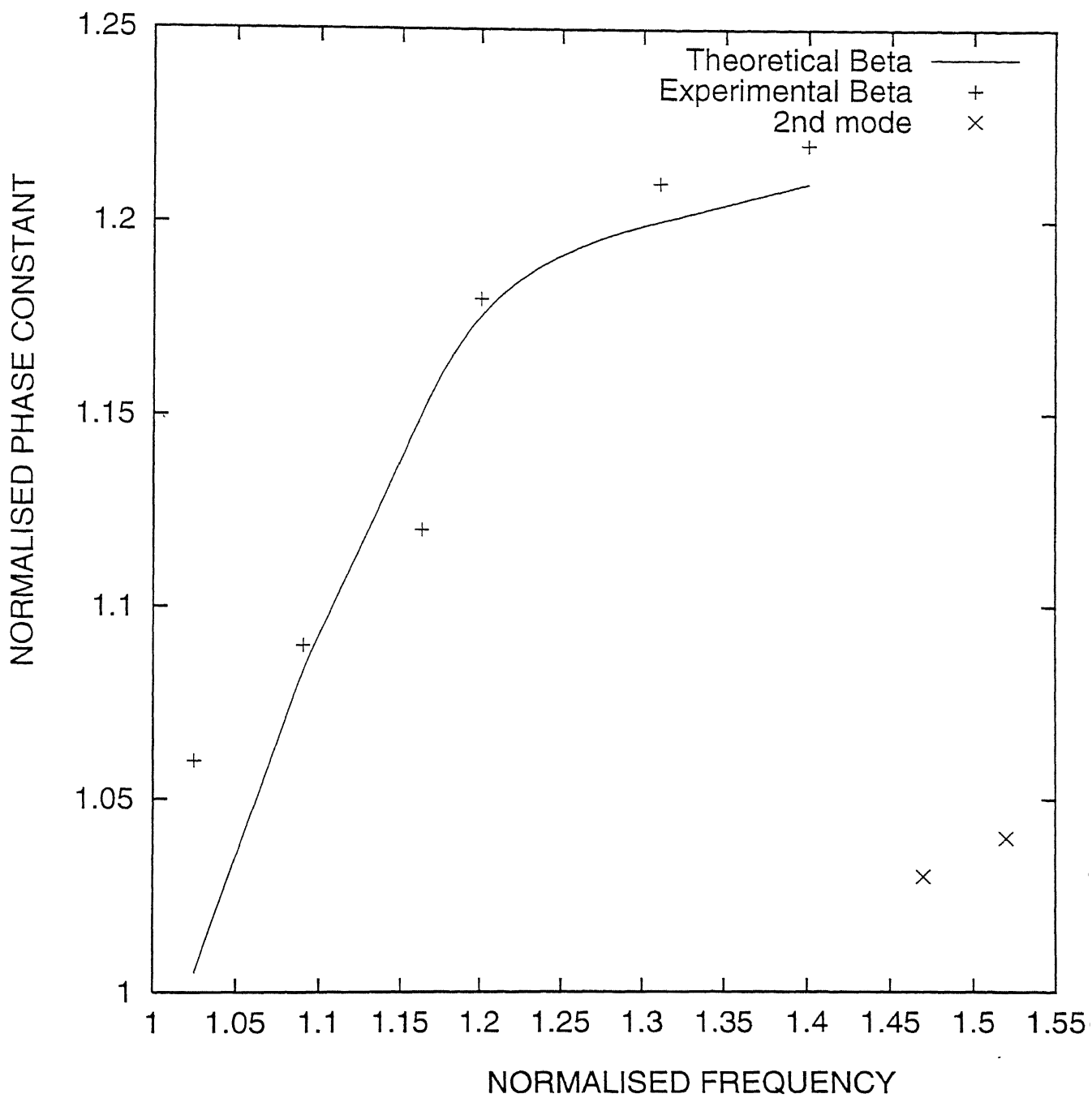


Figure 2.9: COMPARISION OF THEORETICAL AND EXPERIMENTAL PHASE CONSTANT

Chapter 3

CHARACTERISATION OF AIR-GAP TYPE OF DISCONTINUITY

With the experimental set-up enumerated in previous chapters, air-gap type of discontinuity was analysed employing the approach described in section 2.4. As explained earlier, the first requirement was to obtain magnitude and phase of transmission scattering parameter S_{21} of the discontinuity. This was obtained on Network analyser HP8410 and on HP 8510B. The results are as shown from fig 3.1 to fig 3.5. From these S parameter values, series reactance \overline{X}_{se} and shunt reactance \overline{X}_{sh} of equivalent T-network was calculated. One such sample calculation has been shown in succeeding section. The calculated results for \overline{X}_{se} has been given in table 3.1 and those for \overline{X}_{sh} is shown in table 3.2. In fig 3.6 and 3.7 results of \overline{X}_{se} and \overline{X}_{sh} at various frequencies has been plotted against increasing gap width. The same reactance values at air gap discontinuity width of 1 cm, 1.5 cm, 2 cm and 2.5 cm has been plotted against increasing frequencies in fig 3.8 and in fig 3.9.

3.1 A SAMPLE CALCULATION

Since S_{21} was measured on plane of termination of X-band energy launcher, we used equation 2.14 which relates S_{21}^T to even and odd mode resonant length l_e and l_m respectively. Equation 2.14 can also be written separately in real and imaginary parts.

and

$$\overline{X_{sh}} = \frac{-\overline{X_{se}} - j \tan \beta l_m}{2} \quad (3.10)$$

Substituting the values of l_e and l_m as obtained above in equation 3.8, we get,

$$\overline{X_{se}} = -j0.235 \text{ and } \overline{X_{sh}} = -j0.847$$

A tabular representation of all reactance values ($\overline{X_{se}}$ and $\overline{X_{sh}}$) is given in table 3.1 and table 3.2

3.2 ELEMENTARY EXPLANATION OF NORMALISED REACTANCE VALUES RESULTS

A rigorous explanation of discontinuity parameter can only be provided through a detailed theoretical investigation of the same. Since the present work was confined to experimental characterisation of image line discontinuity and in absence of any such previous theoretical investigation, we try to present in succeeding paragraph a brief explanation of the results.

When a wave travelling on image line encounters an abrupt discontinuity, it leads to generation of many higher order modes. Most of these modes are non-propagating in nature and decay down before reaching the other side of the discontinuity. However, even a few of them, which manage to reach other end of the discontinuity, give rise to another set of higher order modes. As the width of air gap type of discontinuity is increased, fewer of such modes are generated, and, in turn, propagated through the length of the image line. We know that, Power = $P_{av} = V^2/Z$, where V is the voltage and Z is the impedance.

Since $P_{av} = \sum_{n=0}^{\infty} V_n I_n^*$ Where n is the number of modes.

hence, Reactance

$$Z = V^2 / \sum_{n=0}^{\infty} V_n I_n^* \quad (3.11)$$

and, admittance

$$Y = I^2 / \sum_{n=0}^{\infty} V_n I_n^* \quad (3.12)$$

If we observe the nature of $\overline{X_{se}}$ in table 3.1 and in fig 3.6, we will find that at all the frequencies of investigation, at 1 cm air-gap width, the reactance is capacitive and, thereafter, it became inductive in nature. Also, we find that at a constant frequency, as the discontinuity width is increasing, the reactance value increases. One possible explanation

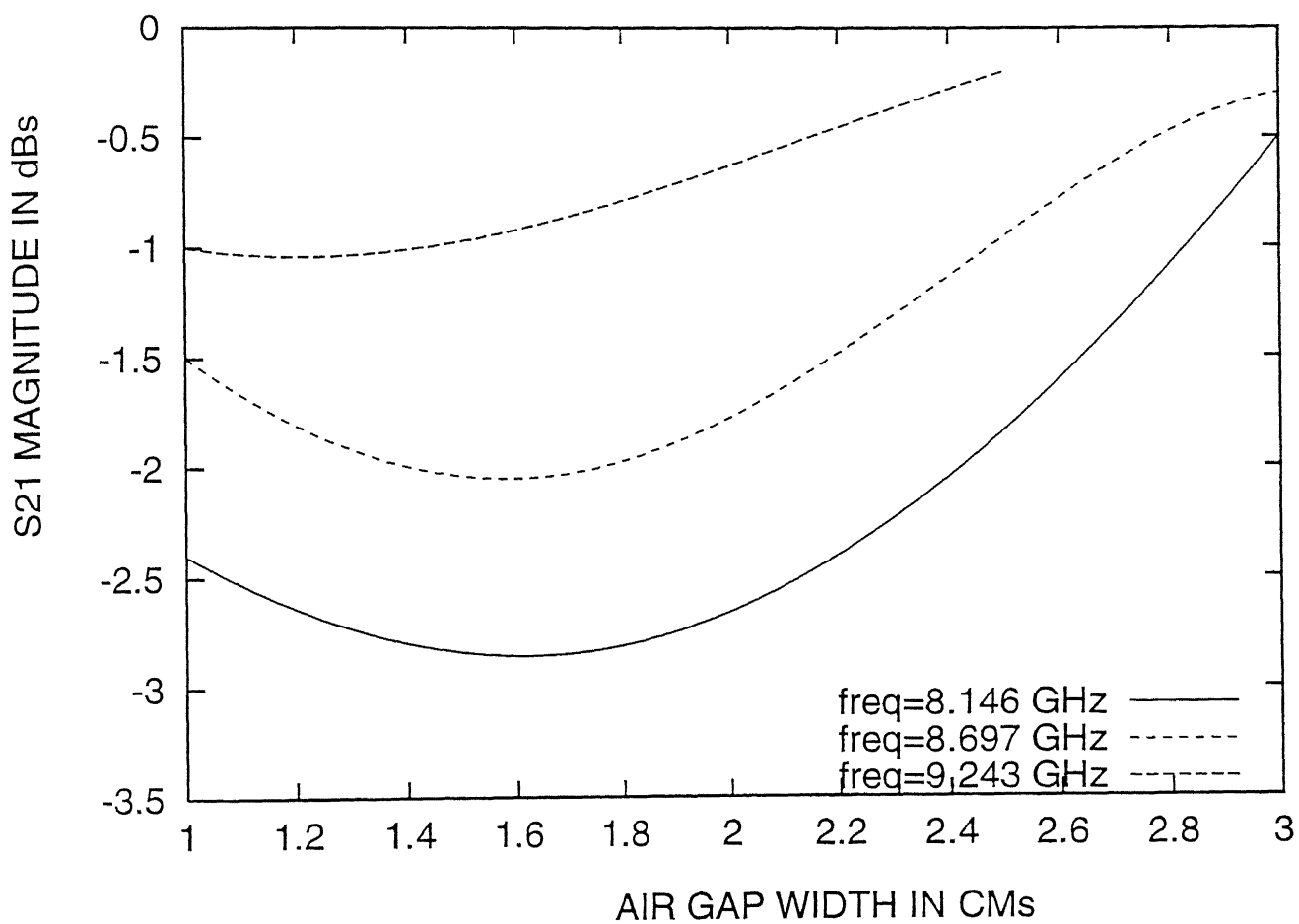


Figure 3.1: S21 MAGNITUDE PARAMETER OF AIR GAP TYPE OF DISCONTINUITY FROM 8.146 - 9.243 GHz

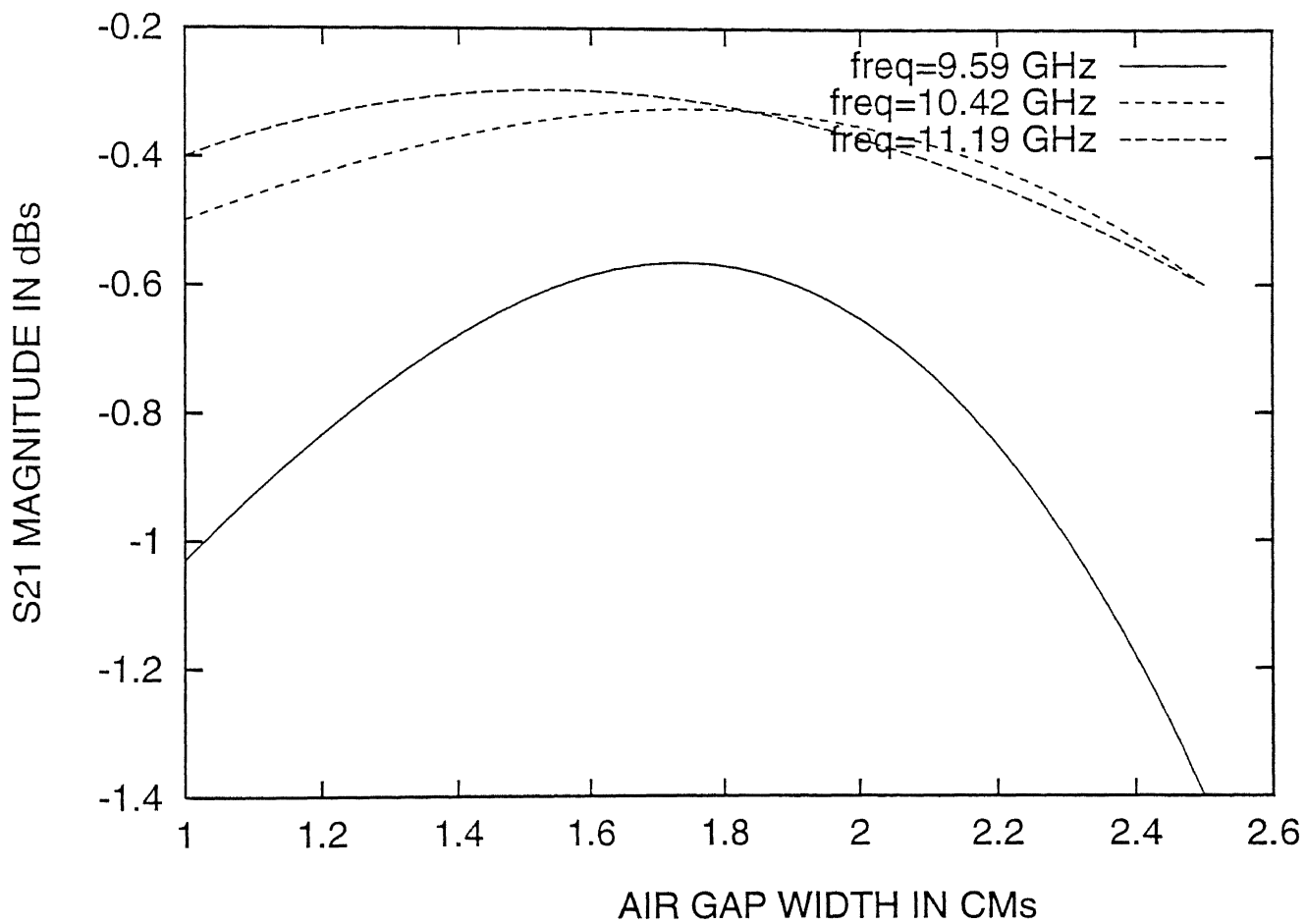


Figure 3 2: S21 MAGNITUDE PARAMETER OF AIR GAP TYPE OF DISCONTINUITY FROM 9.59 - 11.19 GHz

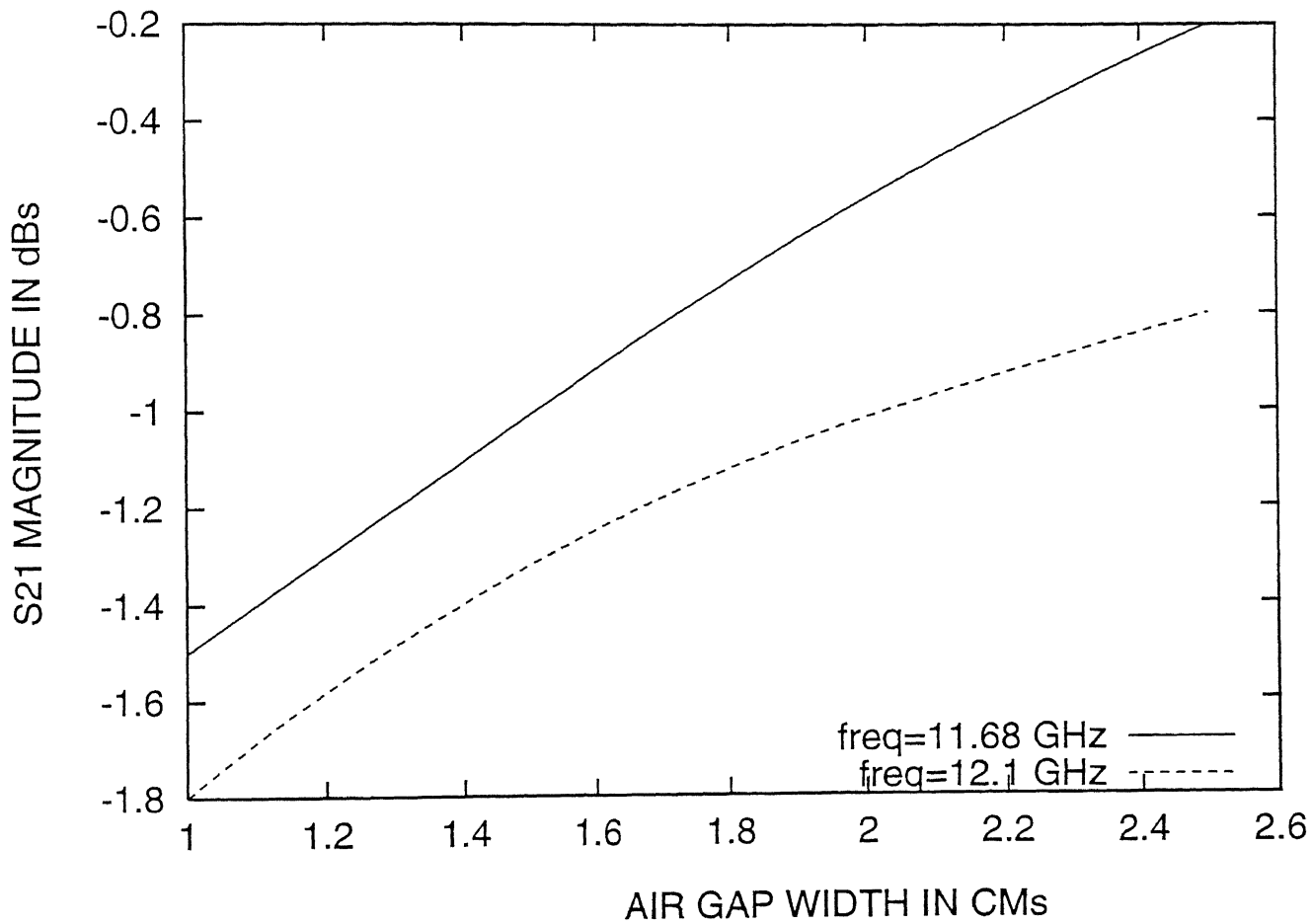


Figure 3.3: S21 MAGNITUDE PARAMETER OF AIR GAP TYPE OF DISCONTINUITY FROM 11.68 -12.1 GHz

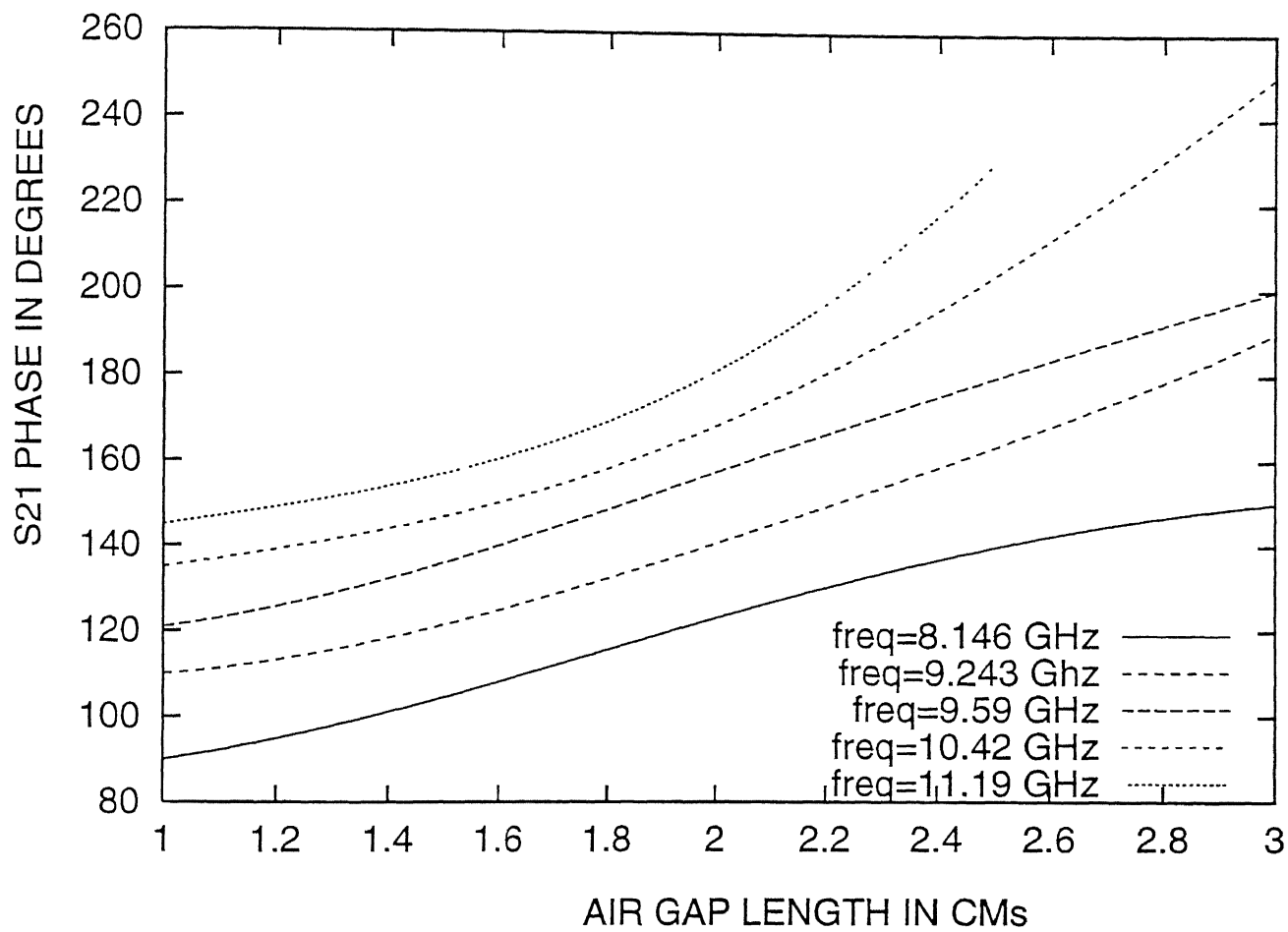


Figure 3.4: S21 PHASE PARAMETER OF AIR GAP TYPE OF DISCONTINUITY FROM 8.146 - 11.19 GHz

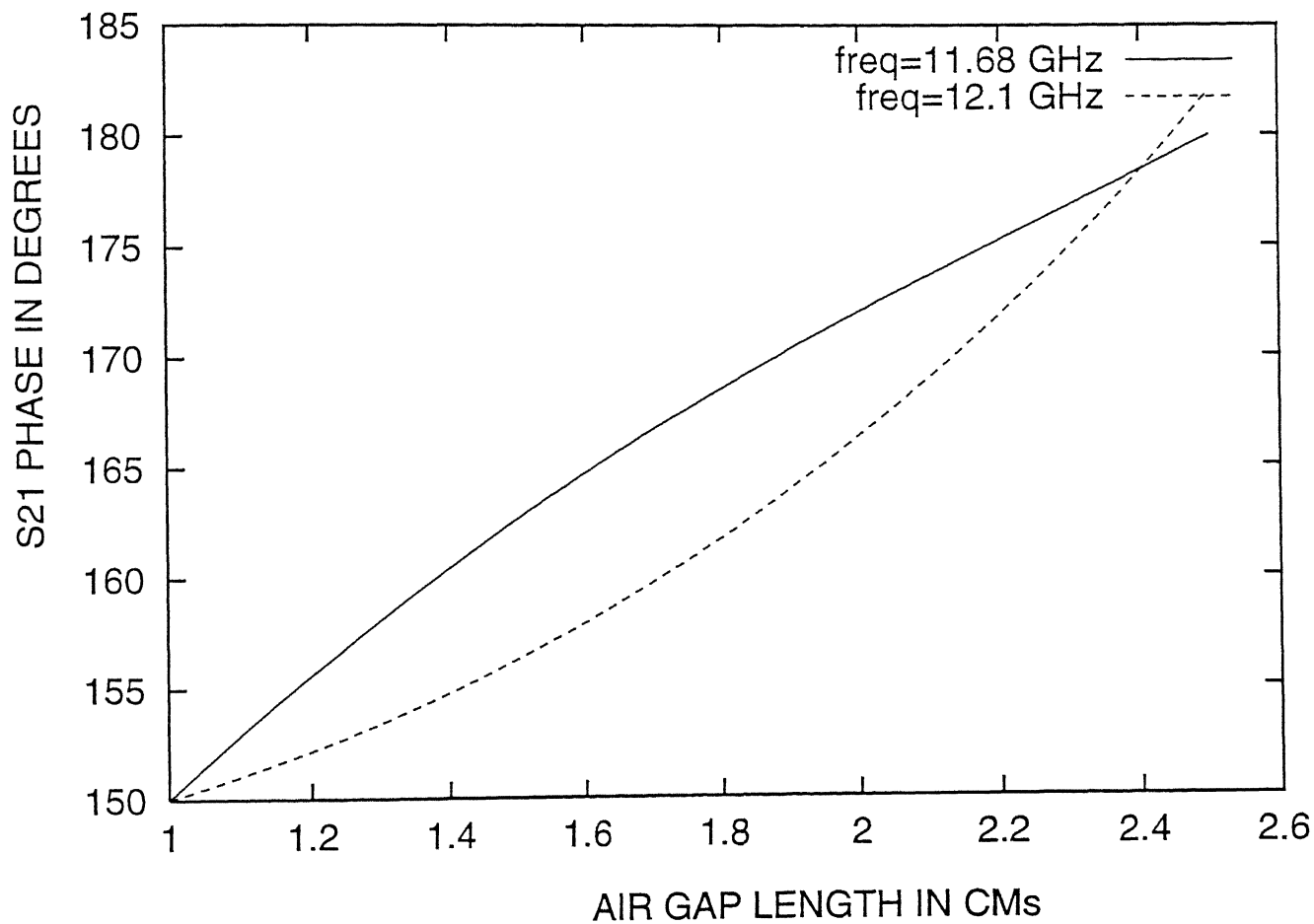


Figure 3.5: S21 PHASE PARAMETER OF AIR GAP TYPE OF DISCONTINUITY FROM 11.68-12.1 GHz

may be that in equation 3.11, as gap discontinuity width increase, number of modes arriving at the other end of the gap discontinuity decreases i.e. n decreases. Hence, reactance Z increases. On the other hand, $\overline{X_{sh}}$ remains capacitive throughout, and, at any constant frequency, it decreases upto 2 cm gap and thereafter it increases. As the discontinuity width increases, number of modes n decreases, which results in increased admittance Y , i.e. reactance Z decreases. However, after the 2 cm gap width the dimensions of the discontinuity being comparable to the wavelength of operation, capacitive reactance of $\overline{X_{sh}}$ gets dictated by parallel plate capacitance phenomenon. $C = \epsilon A/d$ where A is the area and d is the separation between the plates. Here, as gap width increase beyond 2 cm, capacitance C decreases. Hence, capacitive reactance $1/j\omega C$ increases.

If we try to analyse the reactance values for increasing frequency at any constant gap width, we find that in table 3.1, generally $\overline{X_{se}}$ is decreasing as the frequency increases. This may be because of increasing ω in capacitive reactance $1/j\omega C$, other parameters being same at constant gap width. When $\overline{X_{se}}$ becomes inductive in nature after 2 cm gap width, keeping in agreement with inductive reactance $j\omega L$ expression, at a constant gap, when ω increases with increasing frequency, inductive reactance of $\overline{X_{se}}$ increases. Meanwhile, $\overline{X_{sh}}$ observations with increasing frequency at any constant gap width indicates that it is increasing with frequency. It may be explained by the fact that higher frequency means more number of higher order modes n , which, makes admittance Y smaller in equation 3.12 and, in turn, makes reactance increasing in nature.

ser.no.	freq In GHz	air gap length				
		1cm	1.5cm	2cm	2.5cm	3cm
1	8.146	-j0.235	j 0.093	j0.2675	j0.8284	j5.2
2	8.697	-j0.1485	j0.243	j0.579	j1.7416	j6.88
3	9.243	-j0.1294	j0.3507	j0.8548	j2.2925	j7.36
4	9.59	-j0.08	j0.553	j1.28	j2.33	j7.9
5	10.42	-j0.042	j0.709	j2.76	j 6.85	j12.9
6	11.19	-j0.046	j0 9585	j4.15	j8.033	
7	11.68	-j0 341	j0.2356	j1.165		
8	12.10	-j0.3116	j 0.3849	j1.4843		

Table 3.1: NORMALISED SERIES REACTANCE VALUES OF EQUIVALENT T-NETWORK MODEL OF AIR GAP DISCONTINUITY

ser.no.	freq In GHz	air gap length				
		1cm	1.5cm	2cm	2.5cm	3cm
1	8.146	-j0.847	-j0.453	-j0 3	-j0.54	-j2.52
2	8.697	-j1.033	-j0.47	-j0.456	-j0.9645	-j1.92
3	9.243	-j1.344	-j0.6137	-j0.6981	-j1.246	-j2.6216
4	9.59	-j1.3852	-j0.703	-j0.8817	-j1.3091	-j1.37
5	10.42	-j1.448	-j0.7693	-j1.45	-j3.31	
6	11.19	-j1.488	-j0.8165	-j2.066	-j3.895	
7	11.68	-j1.8586	-j0.7295	-j0.7782		
8	12.1	-j1.354	-j0.6049	-j0.8041		

Table 3.2: NORMALISED SHUNT REACTANCE VALUES OF EQUIVALENT T-NETWORK MODEL OF AIR GAP DISCONTINUITY

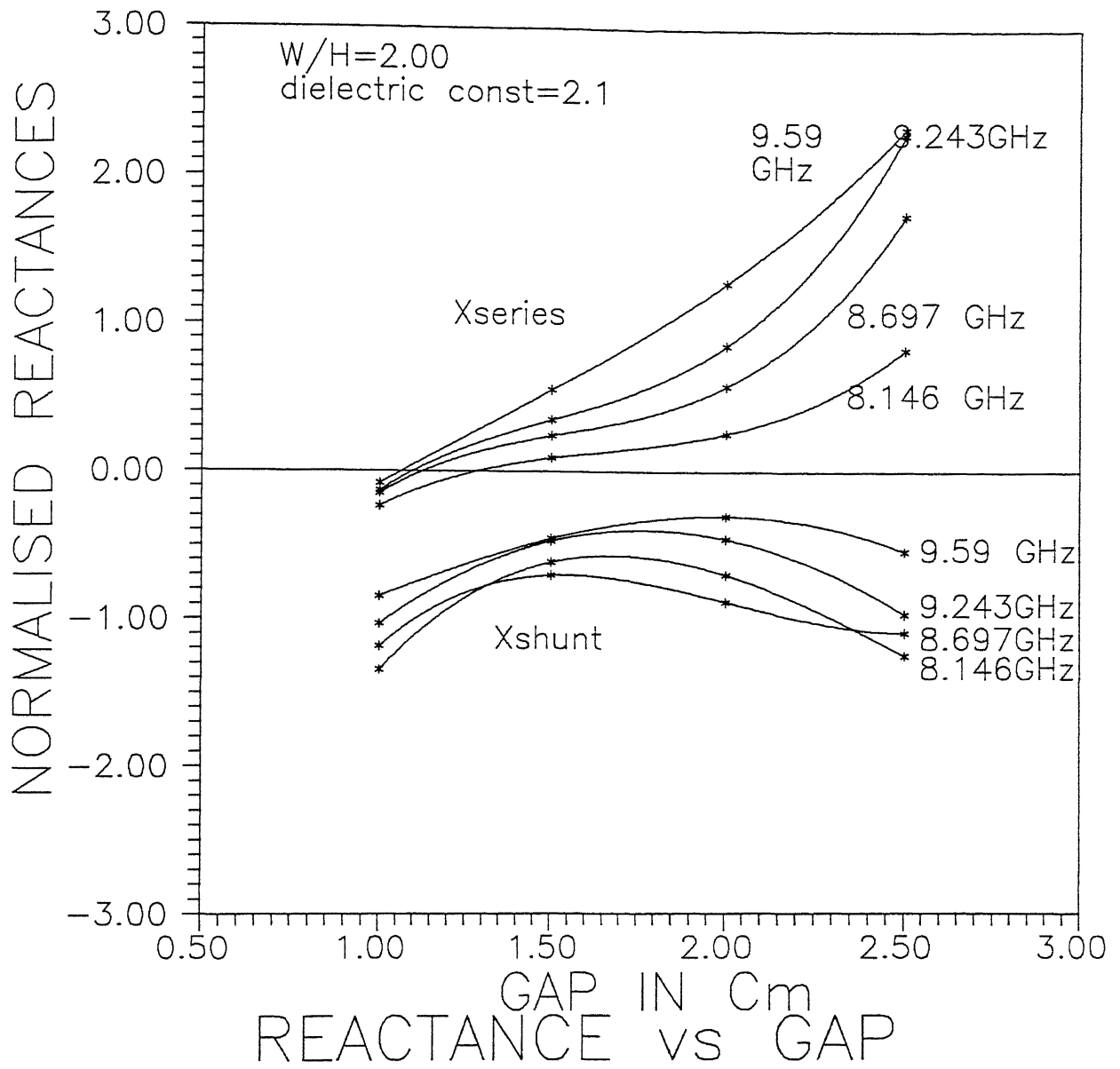


Figure 3-6

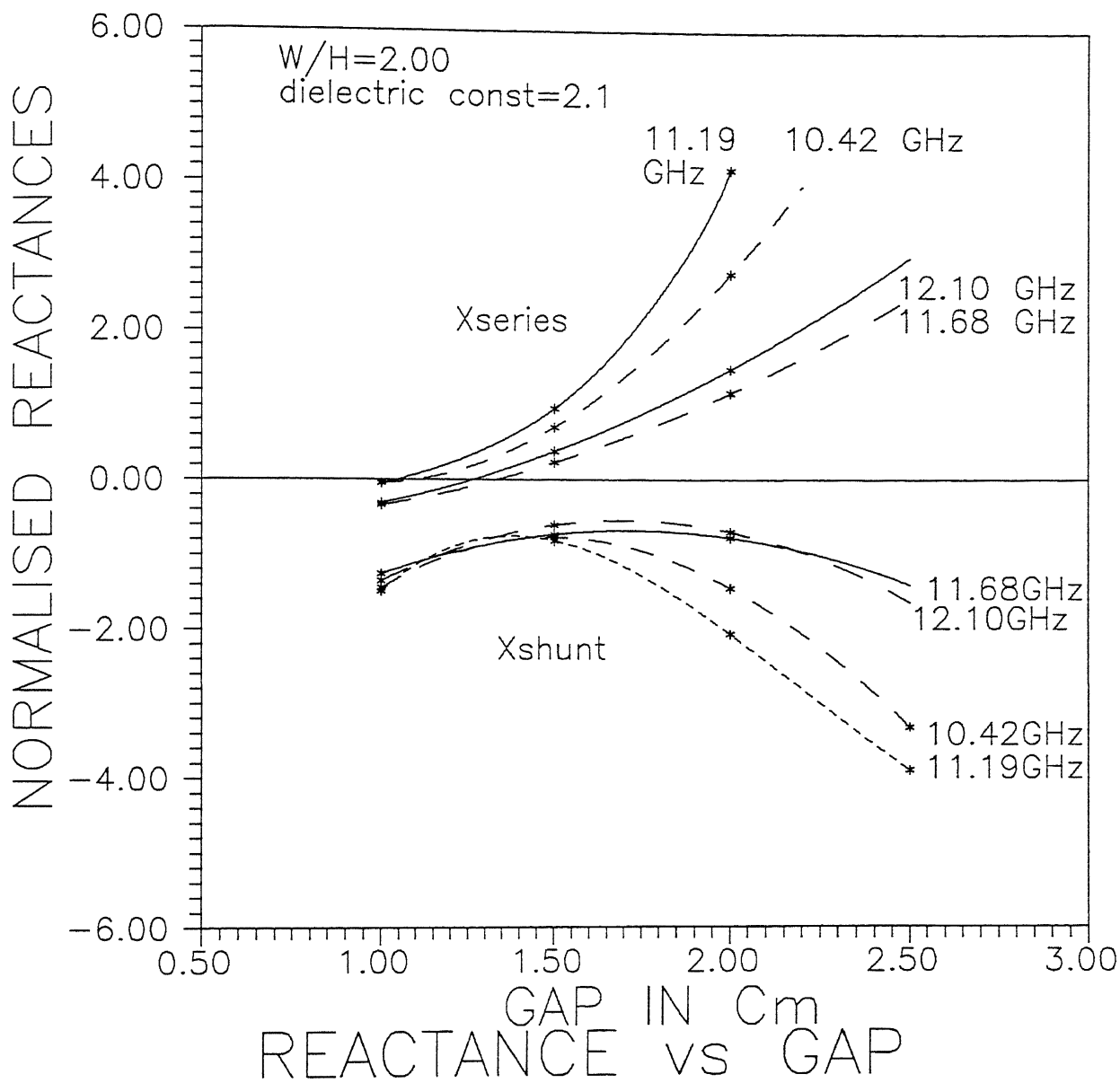


Figure 3.7

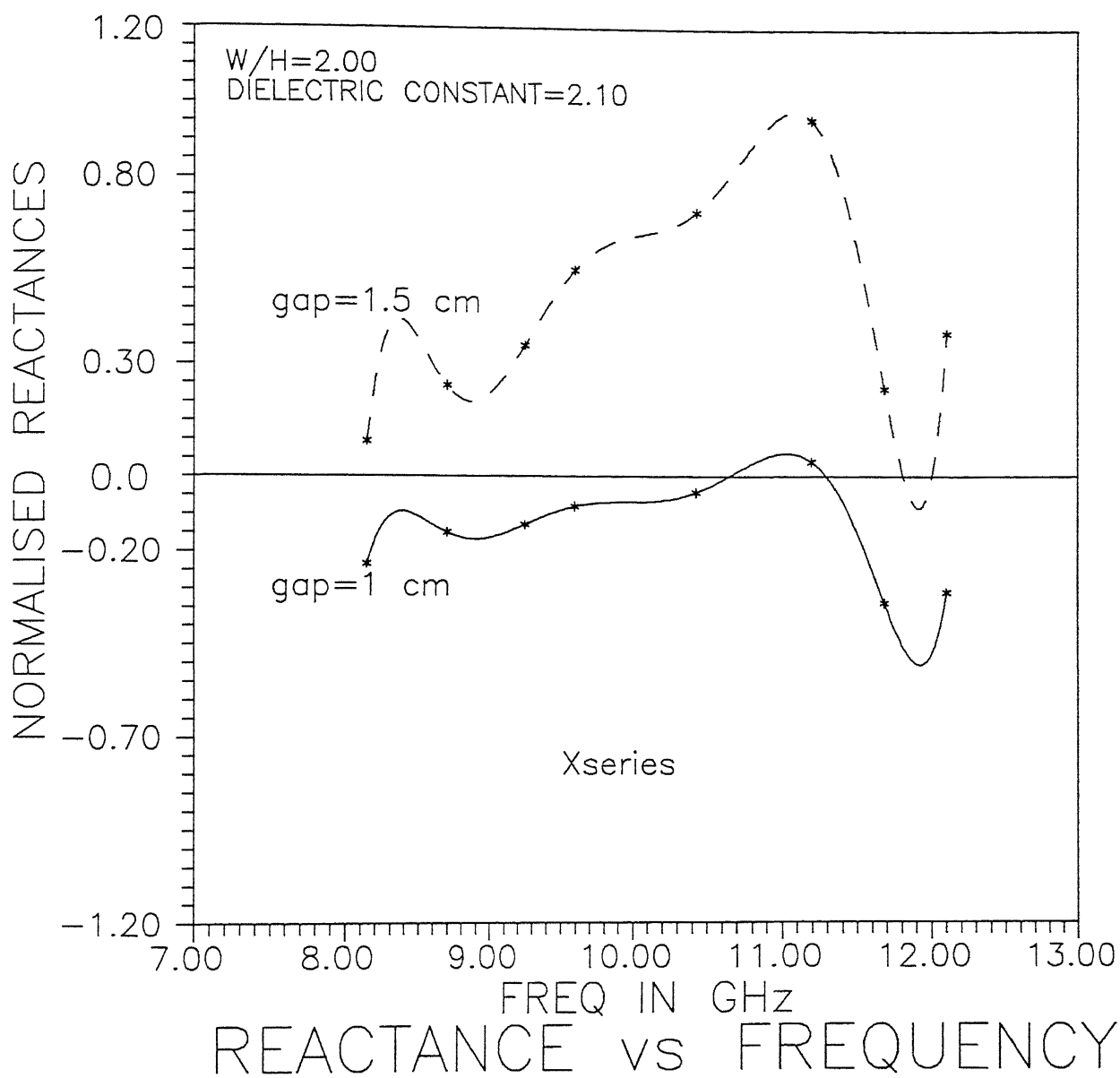


Figure 3-8

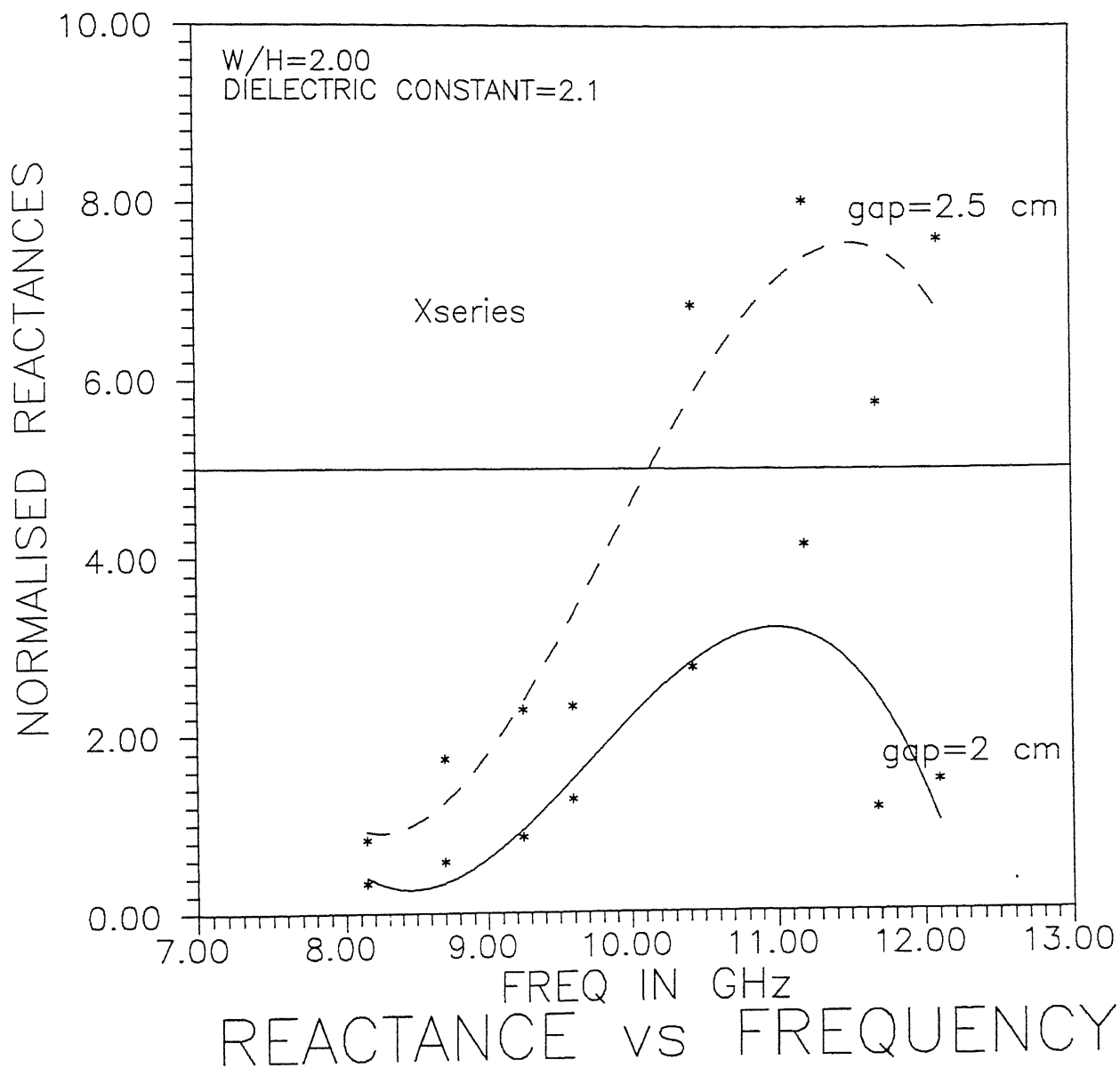


Figure 3-9

Chapter 4

CHARACTERISATION OF NOTCH TYPE OF DISCONTINUITY

Notch type of discontinuity ,as shown in fig 2.7(d), was analysed by adopting methods identical to those employed for air-gap type of discontinuity. Initially, following dimensions were taken for experimental measurement:-

- Length of the line=15.4 cm.
- Aspect ratio=2:1.
- Width of the notch=0.5 cm.

Measurements were taken for notch width starting from 0.5 cm upto 2.5 cm. As explained earlier ,initially, transmission S parameter was measured on network analyser, and subsequently, reactance parameters of equivalent T-network model of notch discontinuity was calculated. Results of S21 observations has been shown from fig 4.1 to fig 4.5 .A sample calculation has been shown in succeeding section. Fig 4.5 and fig 4 6 depict the variation of $\overline{X_{se}}$ with increasing notch width and fig 4.7 - fig 4.8 show the changing nature of $\overline{X_{sh}}$ with the same. From fig 4.9 to fig 4.12 the variation of $\overline{X_{se}}$ and $\overline{X_{sh}}$ with increasing frequency at different notch widths has been produced.

4.1 A SAMPLE CALCULATION

Since S21 was measured on plane of termination of X-band energy launcher, we used equation 2.14 which relates S_{21}^T to even and odd mode resonant length l_e and l_m respectively. Equation 2.14 can also be written separately in real and imaginary parts.

The real part is

$$S_{21}^T(\text{magnitude}) = \sin[\beta(l_e - l_m)] \quad (4.1)$$

and the imaginary part is

$$S_{21}^T(\text{phase}) = \beta(l_e + l_m + 2s) + 90^\circ \quad (4.2)$$

Here we take example to illustrate calculations at freq=8.146 GHz and gap length=0.5 cm.

At this frequency $S_{21}^T = -0.8 \text{ dB}, 70^\circ$

Equating real part which is magnitude of S21 with equation 4.1, we get,

$$10^{-0.8/20} = \sin\beta(l_e - l_m) \quad (4.3)$$

Since $\sin(180 - \theta) = \sin\theta$, we get,

$$l_e - l_m = 114.21/\beta \quad (4.4)$$

Here, $\beta = 104.16$ degrees per cm, so,

$$l_e - l_m = 1.096 \quad (4.5)$$

Now comparing the imaginary part which is equating eqn 4.2 with phase of S21, we get,

$$S_{21}(\text{phase}) = 90 + \beta(l_e + l_m + 2s) - 5 * 360 \quad (4.6)$$

Since $2s=0.5$ cm, we get,

$$l_e + l_m = 16.589 \quad (4.7)$$

Solving equation 4.5 and 4.7, we get,

$$l_e = 8.842, l_m = 7.746 \quad (4.8)$$

Now using equation 4.2 and 4.3, we have,

$$\overline{X_{se}} = -j \tan \beta l_e \quad (4.9)$$

and

$$\overline{X_{sh}} = \frac{-\overline{X_{se}} - j \tan \beta l_m}{2} \quad (4.10)$$

Substituting the values of l_e and l_m as obtained above in equation 4.8, we get,

$$\overline{X_{se}} = -j0.384 \text{ and } \overline{X_{sh}} = -j8.817$$

A tabular representation of all reactance values ($\overline{X_{se}}$ and $\overline{X_{sh}}$) is given in table 4.1 and table 4.2

4.2 COMPARISON OF SCATTERING PARAMETERS AND REACTANCE VALUES OF T-NETWORK MODEL FOR AIR-GAP AND NOTCH TYPE OF DISCONTINUITY

A comprehensive observation of scattering parameter of both type of discontinuity indicates that power transmitted by the image line decreases gradually as discontinuity length increases. This assumption appears to be justified in the general sense, since coupling of fields from one side to the other side of the discontinuity will reduce as the discontinuity length increases. There are departures from this general pattern in the case of air gap, particularly at the higher gap lengths, which may be due to the propagation of some other higher order modes becoming possible. Also, generally, an image line with a notch type of discontinuity, appears to be capable of transmitting more power than an image line having comparable air gap type of discontinuity.

When we compare $\overline{X_{se}}$ and $\overline{X_{sh}}$ results for both air gap and notch type of discontinuity, following trends emerges:-

- $\overline{X_{se}}$ is a capacitive reactance for air gap type of discontinuity at/upto 1 cm discontinuity length and upto 1.5/2.0 cm lengths for notch type of discontinuity. Thereafter, in both the cases it changes to become inductive in nature. A review of table 3.1 and 4.1 along with related plots in fig 3.6-3.3.7 to 4.5-4.6 shows that $\overline{X_{se}}$, for both the type of discontinuities starts from a low negative value (capacitive reactance), constantly increases, crosses the zero reactance value (point of resonance, where capacitive and inductive reactances are equal) and becomes positive (inductive reactance).

- $\overline{X_{sh}}$ remains capacitive in nature for all the discontinuity lengths for all the frequencies in both the cases of air gap and notch discontinuities. A perusal of fig 3.6-3.7 (for $\overline{X_{sh}}$ only) and fig 4.7-4.8 shows that $\overline{X_{sh}}$ increase with increasing discontinuity lengths.
- In fig 3.8-3.9 and in fig 4.9 $\overline{X_{se}}$ has been plotted against frequency at various discontinuity lengths which indicates identical nature of variations of these parameters in both the cases. In fig 4.10-4.12 $\overline{X_{sh}}$ has been plotted against changing frequency at various notch discontinuity lengths.

ser no.	freq In GHz	air gap length				
		0.5cm	1.0cm	1.5cm	2.0cm	2.5cm
1	8.146	-j0.384	-j0.22	-j0.1982	0.0793	0.49
2	8.697	-j0.466	-j0.26	-j0.15	j0.3055	j0.76
3	9.243	-j0.59	-j0.30	-j0.0586	j0.35	j1.14
4	9.59	-j0.5844	-j0.18	j0.181	j0.70	j1.93
5	10.42	-j0.54	-j0.0984	j0.25	j0.967	j2.11
6	11.19	-j0.527	-j0.0216	j0.4482	j1.5129	j2.31
7	11.68	-j0.8108	-j0.3081	j0.0605	j0.6381	j1.43
8	12.10	-j0.84012	-j0.3171	j0.079	j0.7294	j1.79

Table 4.1. NORMALISED SERIES REACTANCE VALUES OF EQUIVALENT T-NETWORK MODEL OF NOTCH TYPE DISCONTINUITY

ser.no.	freq In GHz	air gap length				
		1cm	1.5cm	2cm	2.5cm	3cm
1	8.146	-j8.817	-j1.533	-j1.045	-j0.5976	-j0.4943
2	8.697	-j6.244	-j1.52	-j0.8049	-j0.5769	-j0.47
3	9.243	-j5.55	-j1.39	-j0.7653	-j0.52	-j1.14
4	9.59	-j5.0547	-j0.7876	-j0.5761	-j0.517	-j0.427
5	10.42	-j3.20	-j0.7047	-j0.5139	-j0.503	-j0.41
6	11.19	-j2.258	-j0.6345	-j0.451	-j0.422	-j0.384
7	11.68	-j5.8803	-j0.8213	-j0.4641	-j0.45	-j0.4
8	12.1	-j4.732	-j0.7577	-j0.4304	-j0.4005	-j0.35

Table 4.2: NORMALISED SHUNT REACTANCE VALUES OF EQUIVALENT T-NETWORK MODEL OF NOTCH TYPE DISCONTINUITY

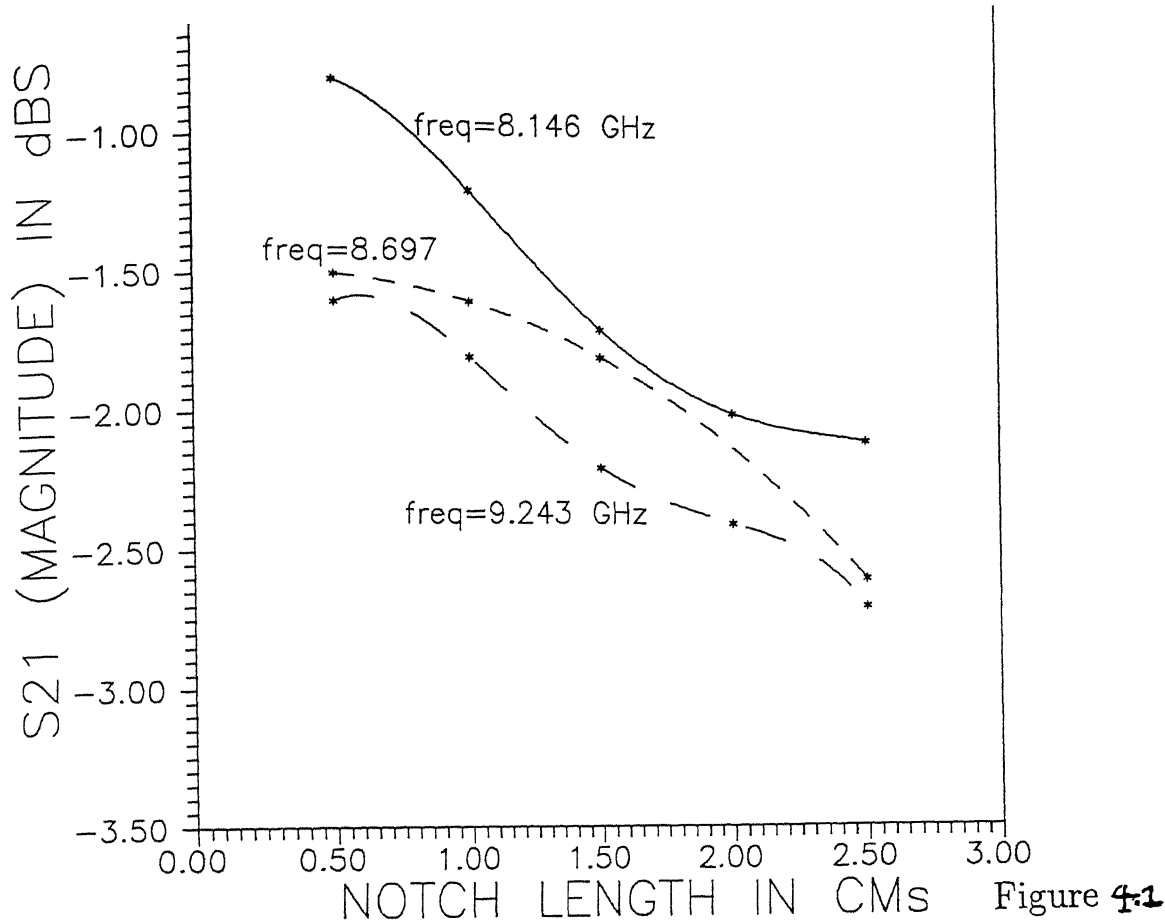


Figure 4.1

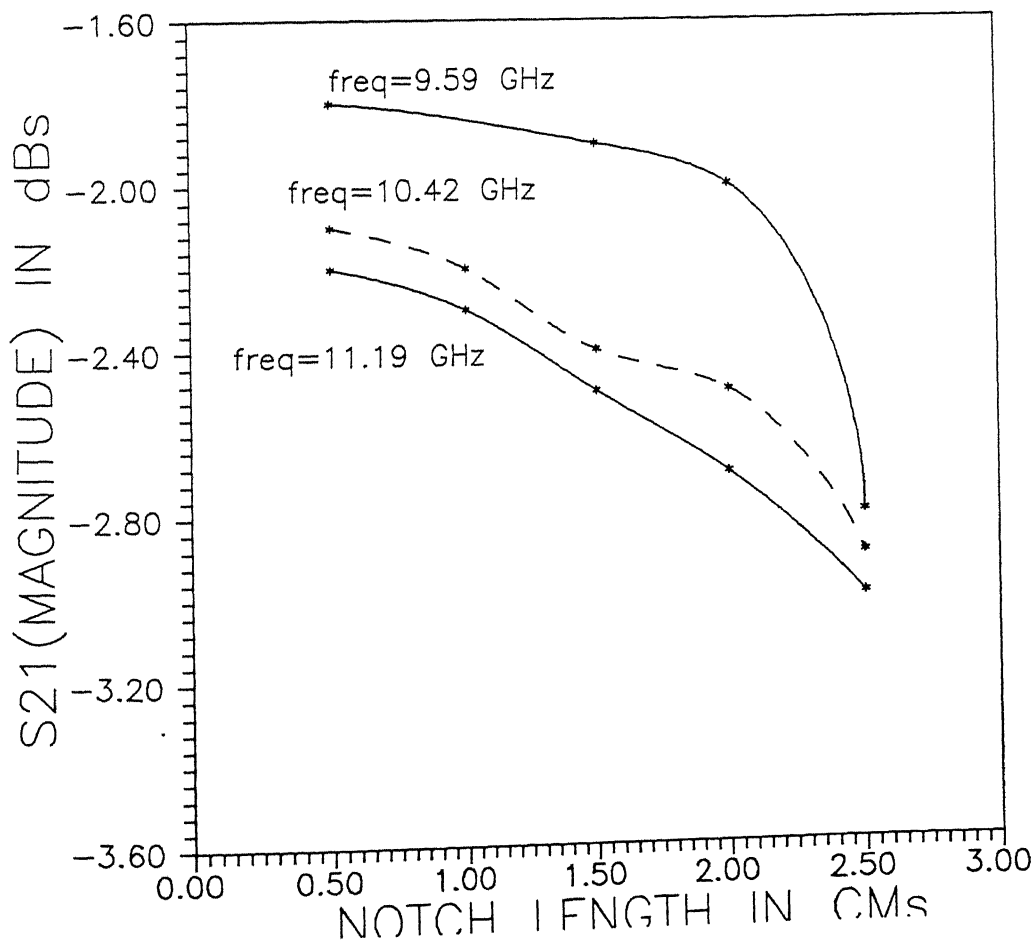


Figure 4.2

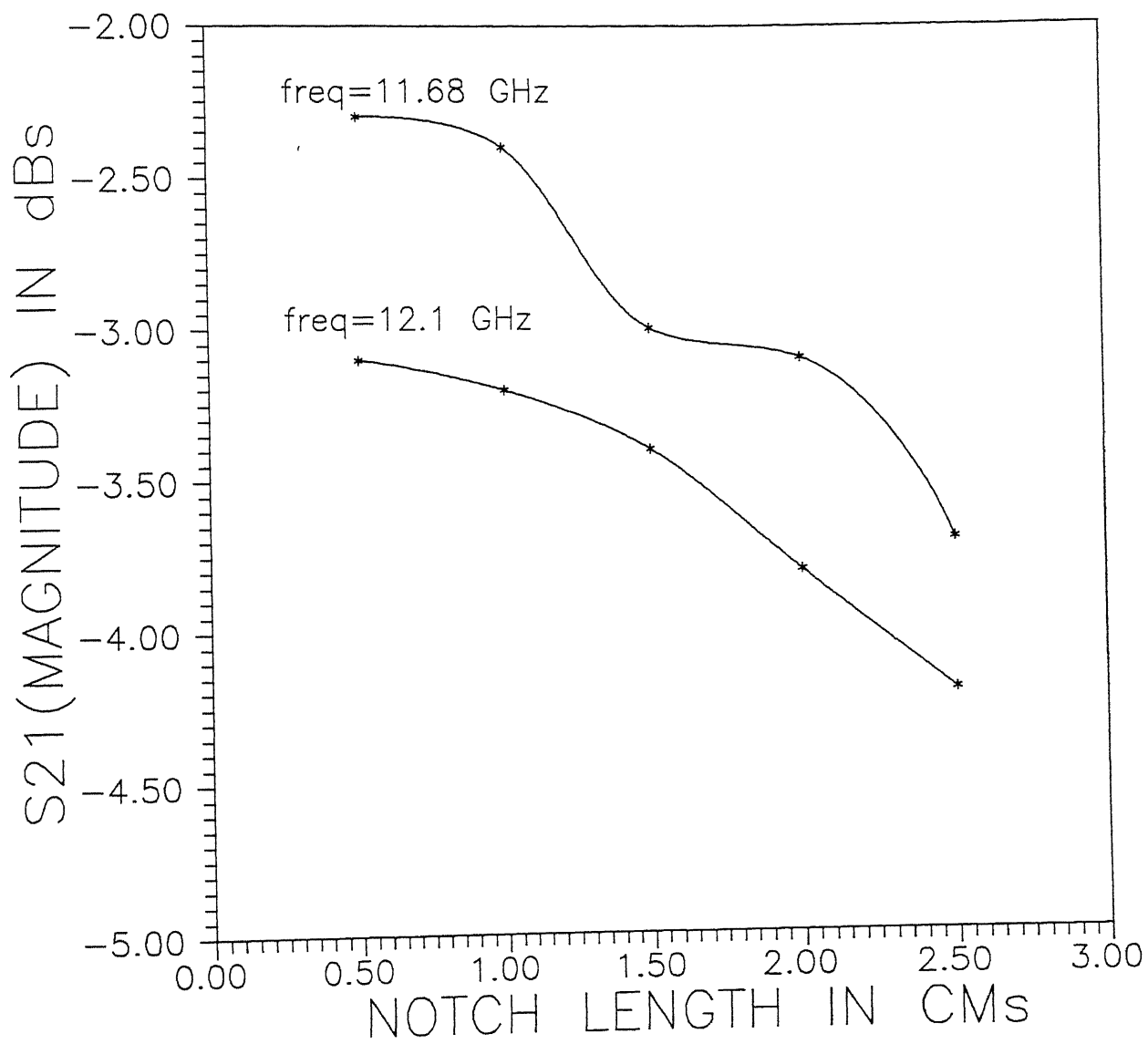


Figure 4-3

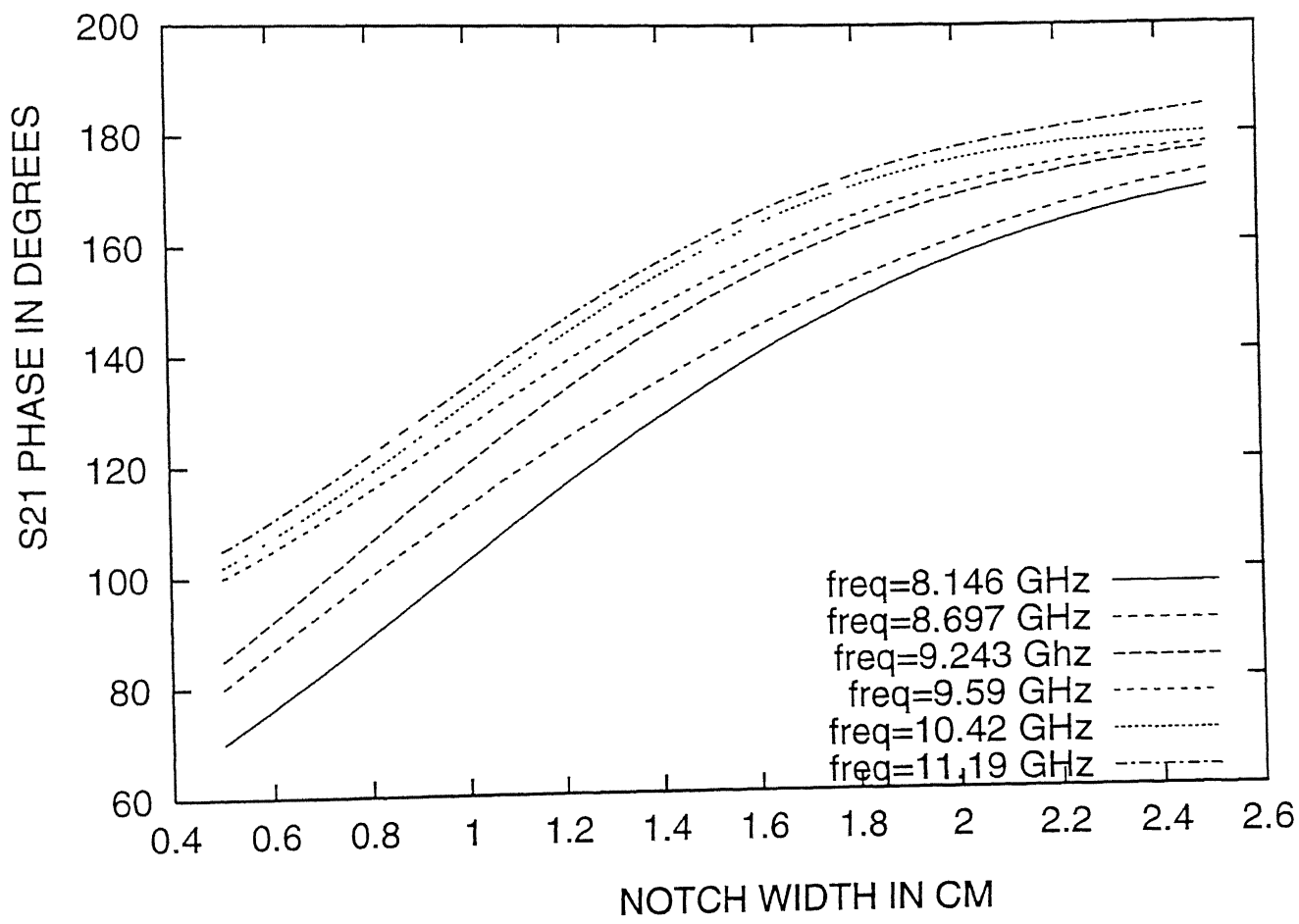


Figure 4.4: S21 PHASE(IN DEGREES) VARIATION WITH CHANGING NOTCH WIDTH

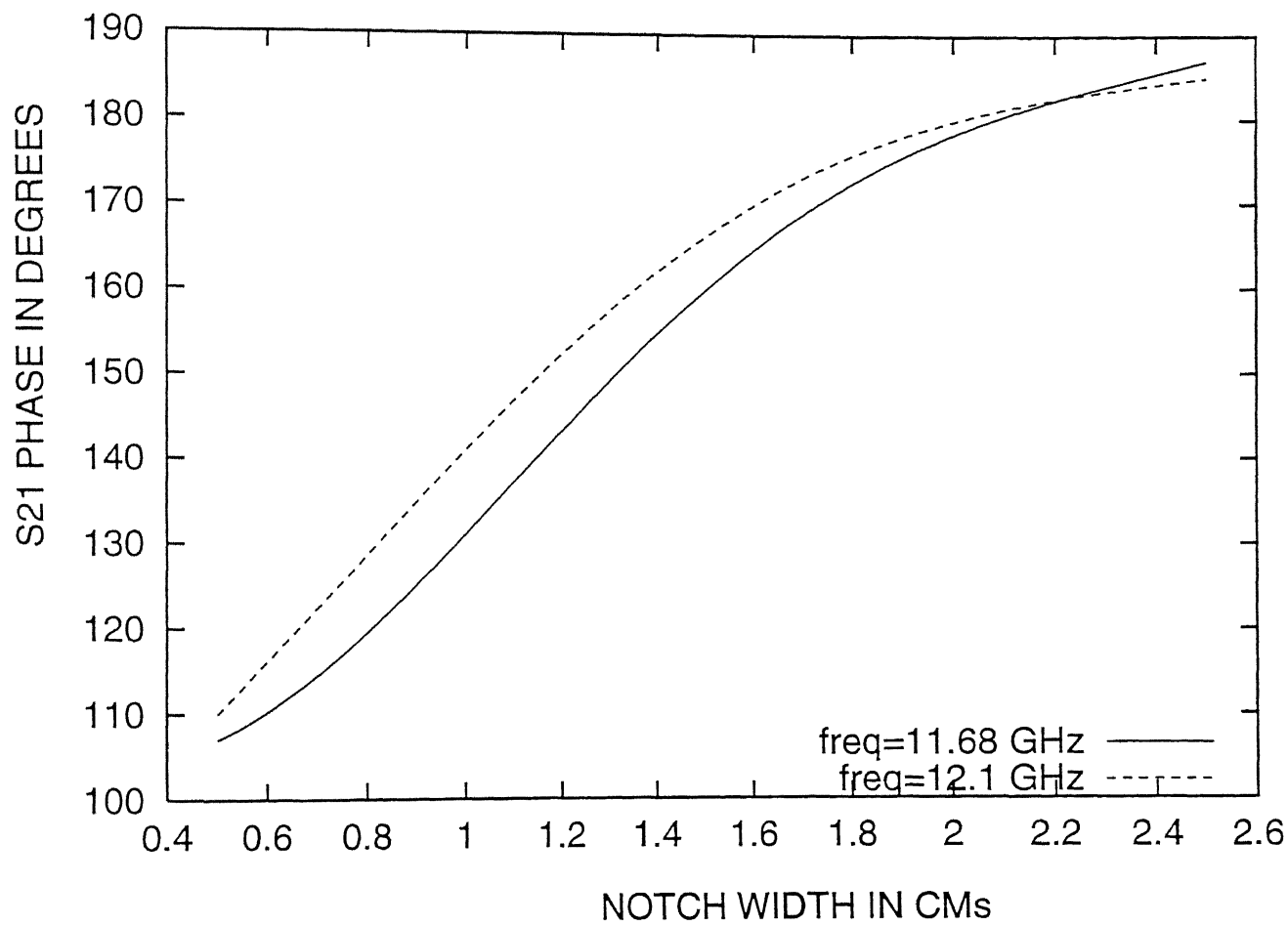


Figure 4.25 S21 PHASE(IN DEGREES) VARIATION WITH CHANGING NOTCH WIDTH

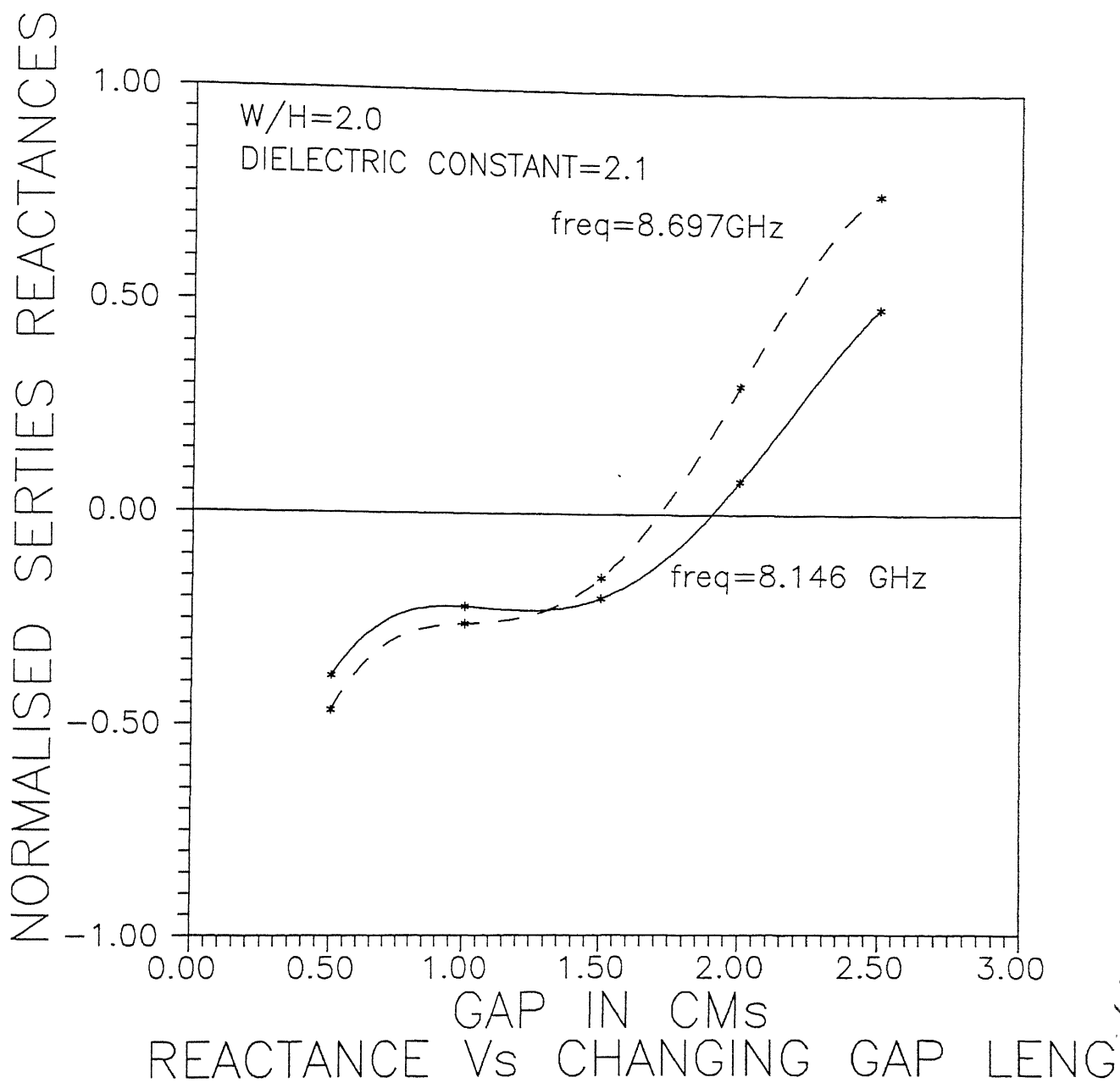


Figure 4.6

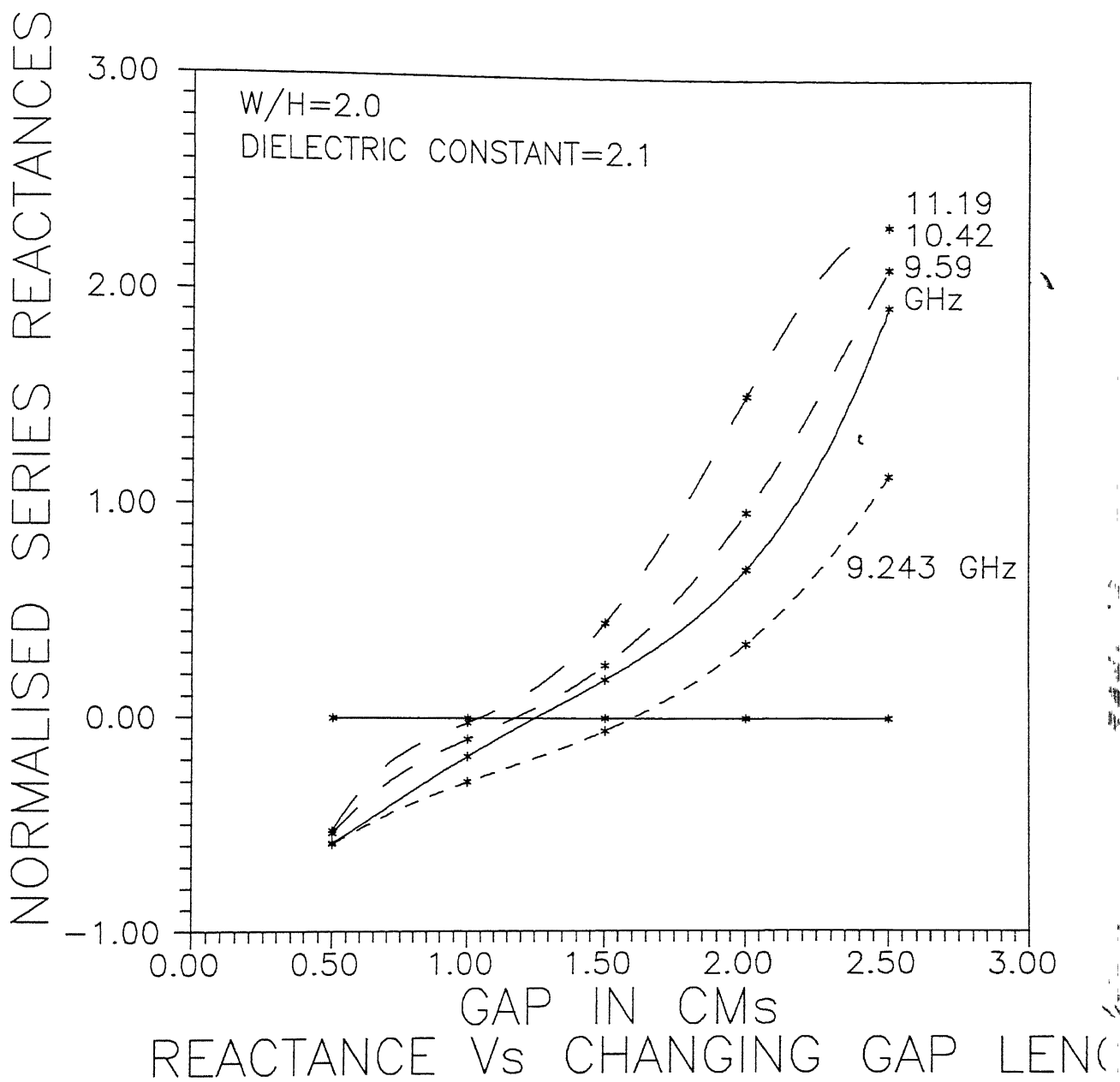


Figure 4.7

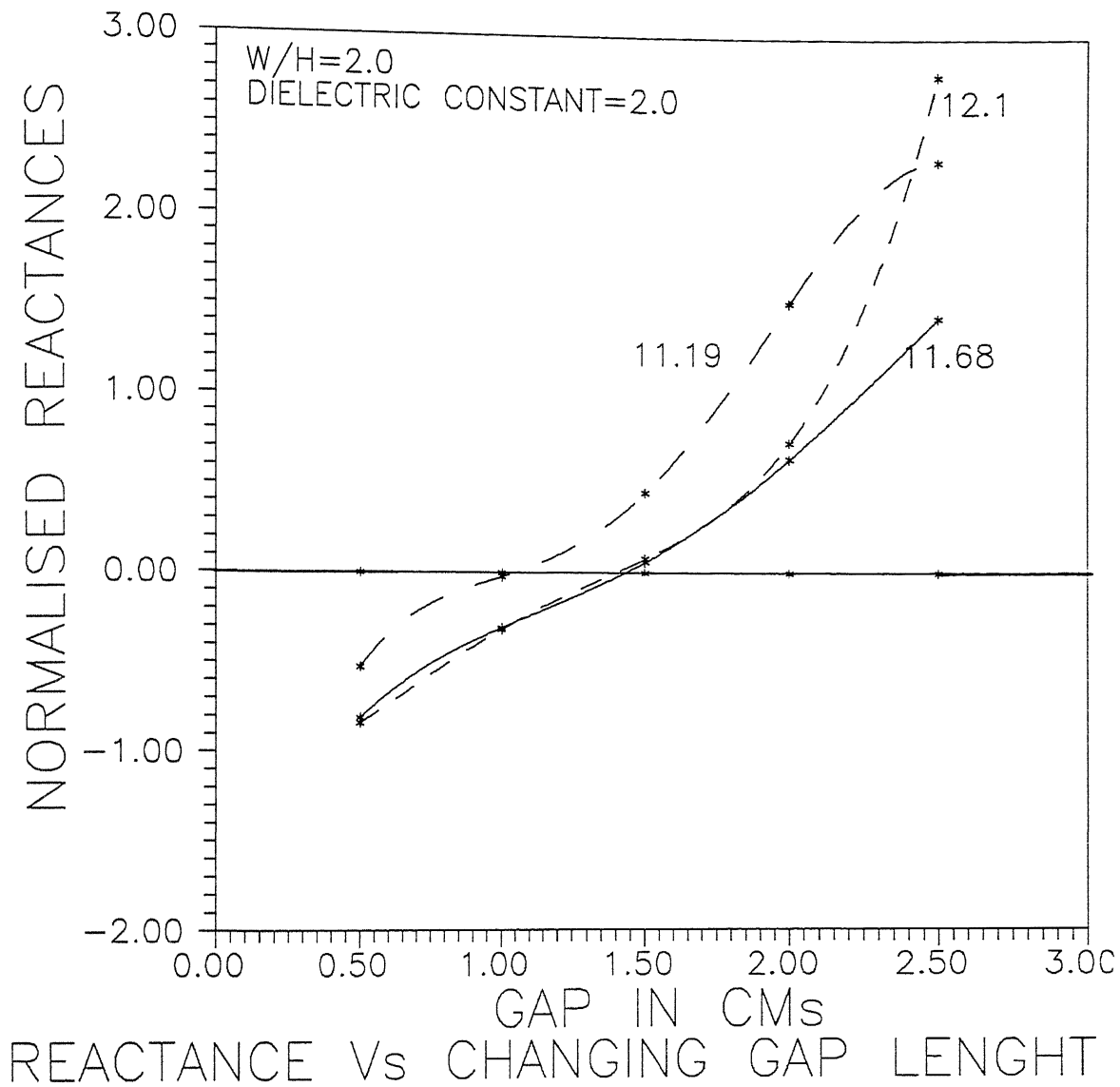


Figure 4-8

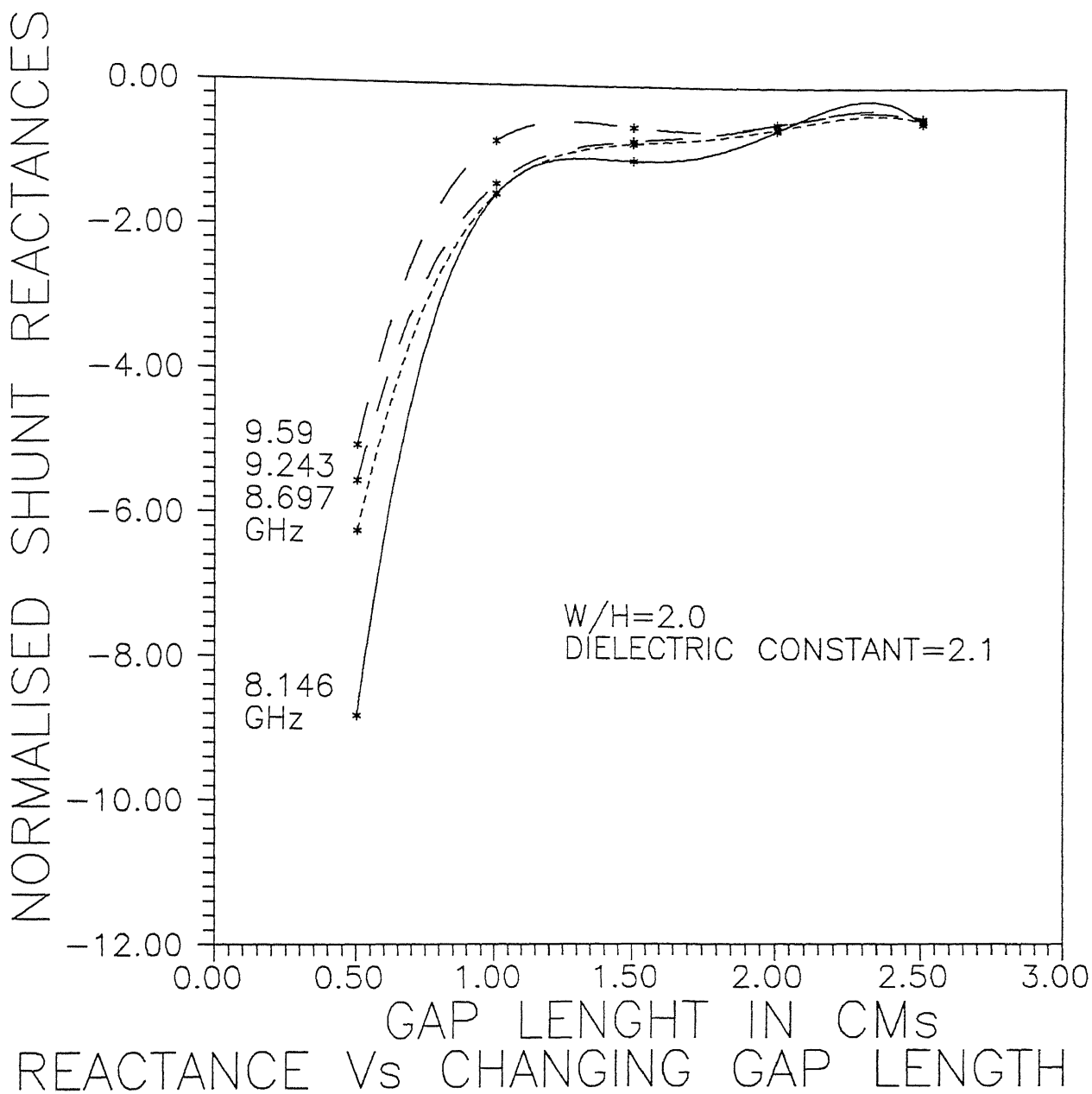


Figure 4.9

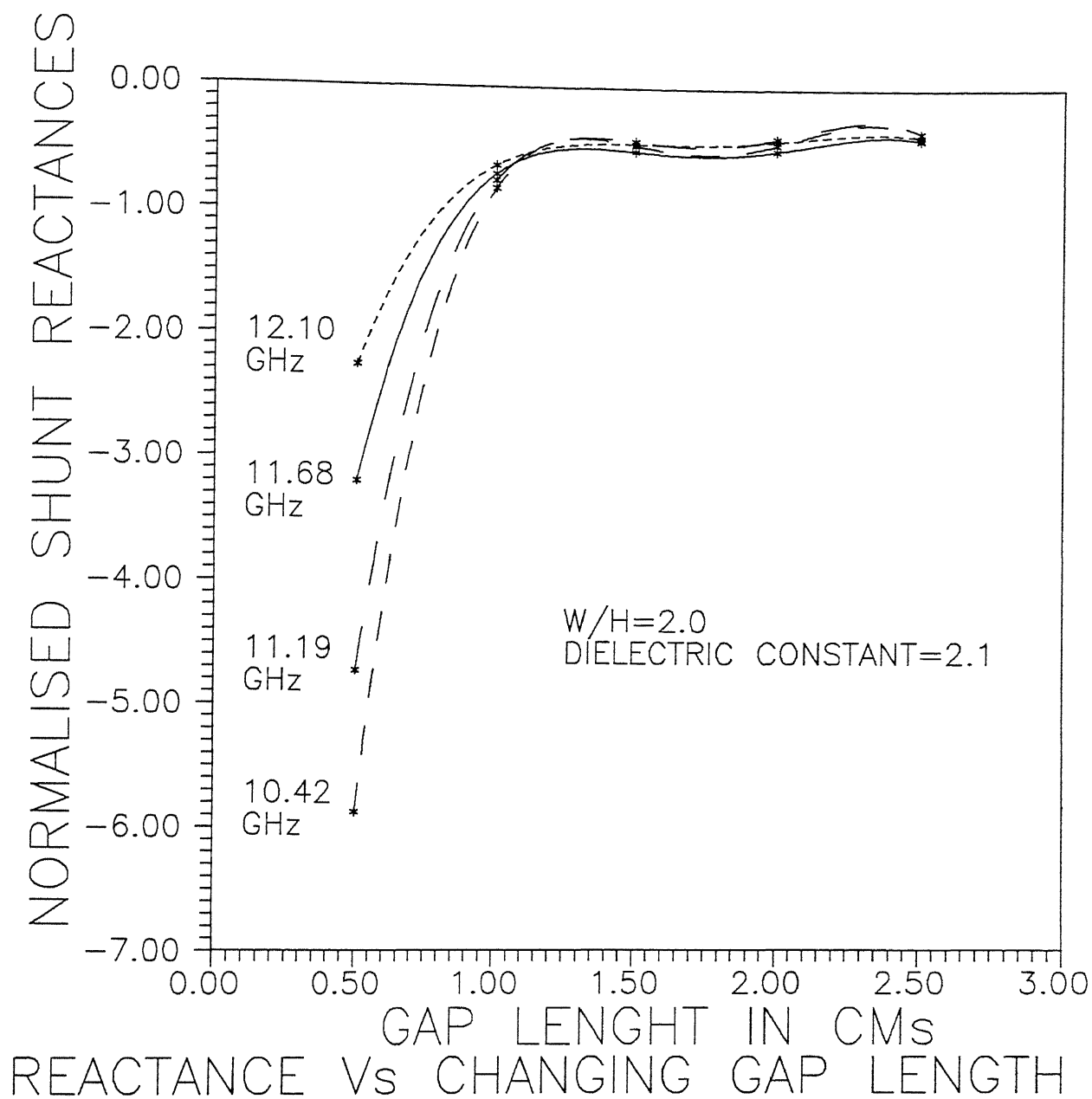


Figure. 4-10

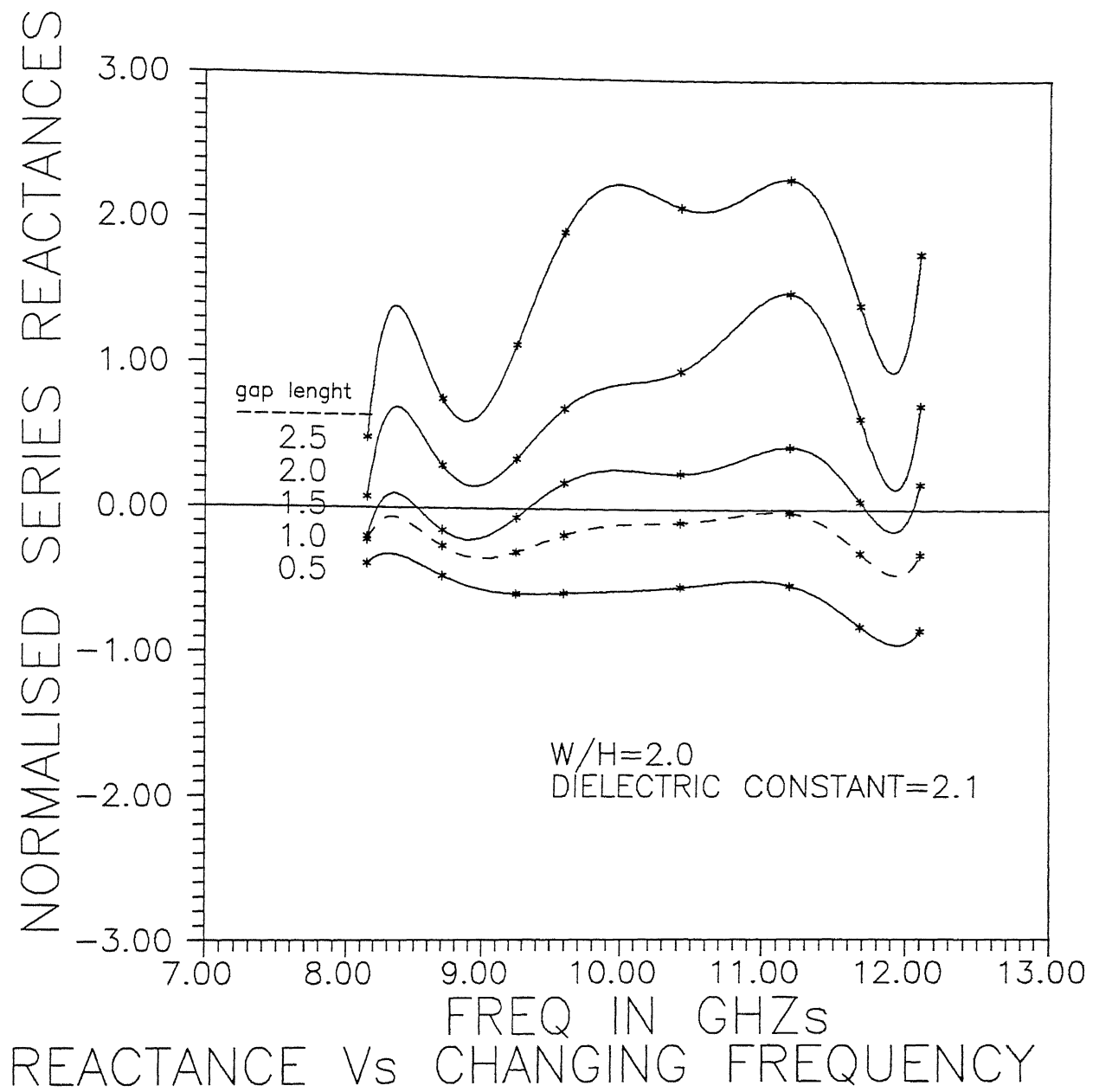


Figure 4.11

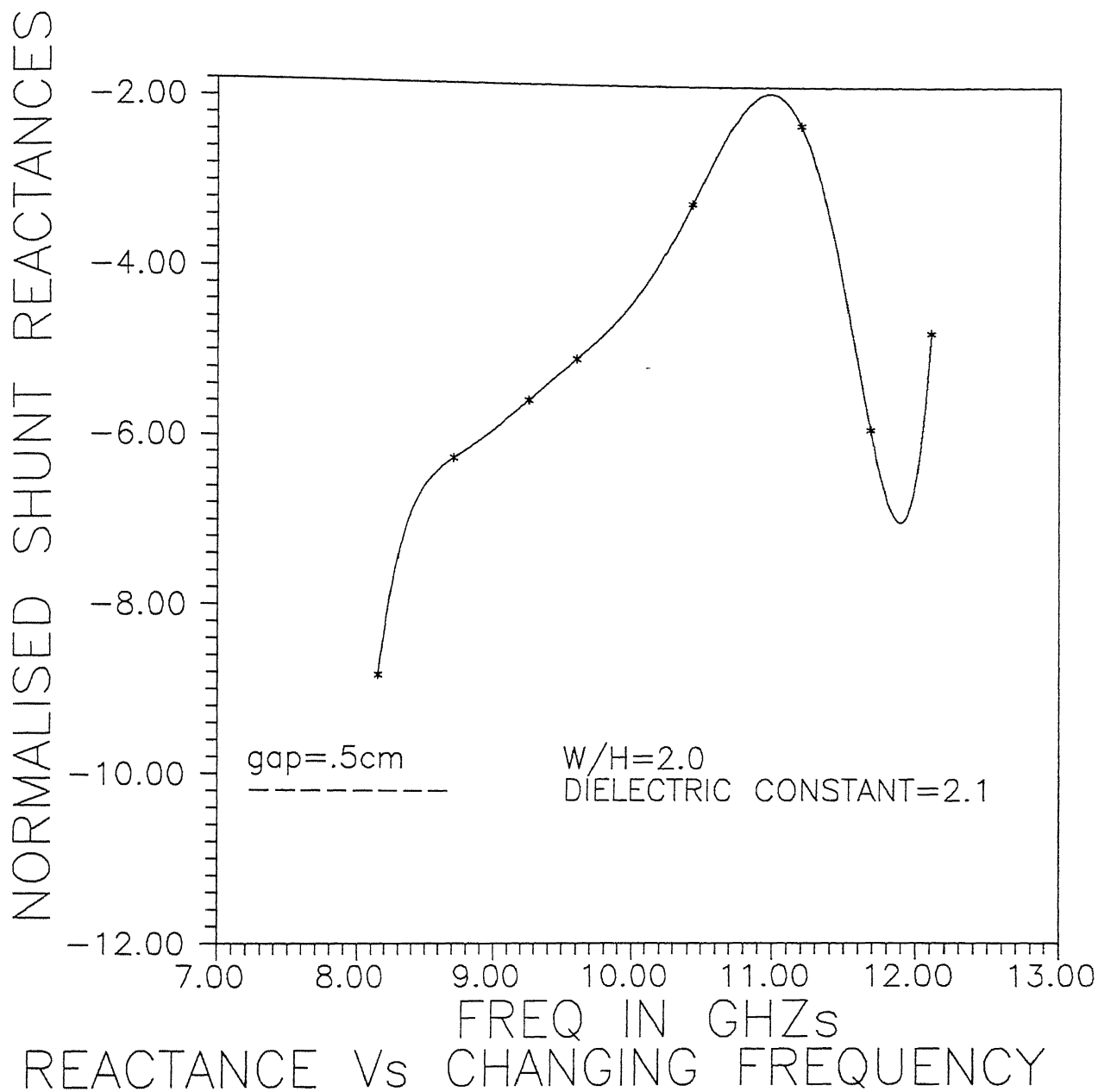


Figure 4.12

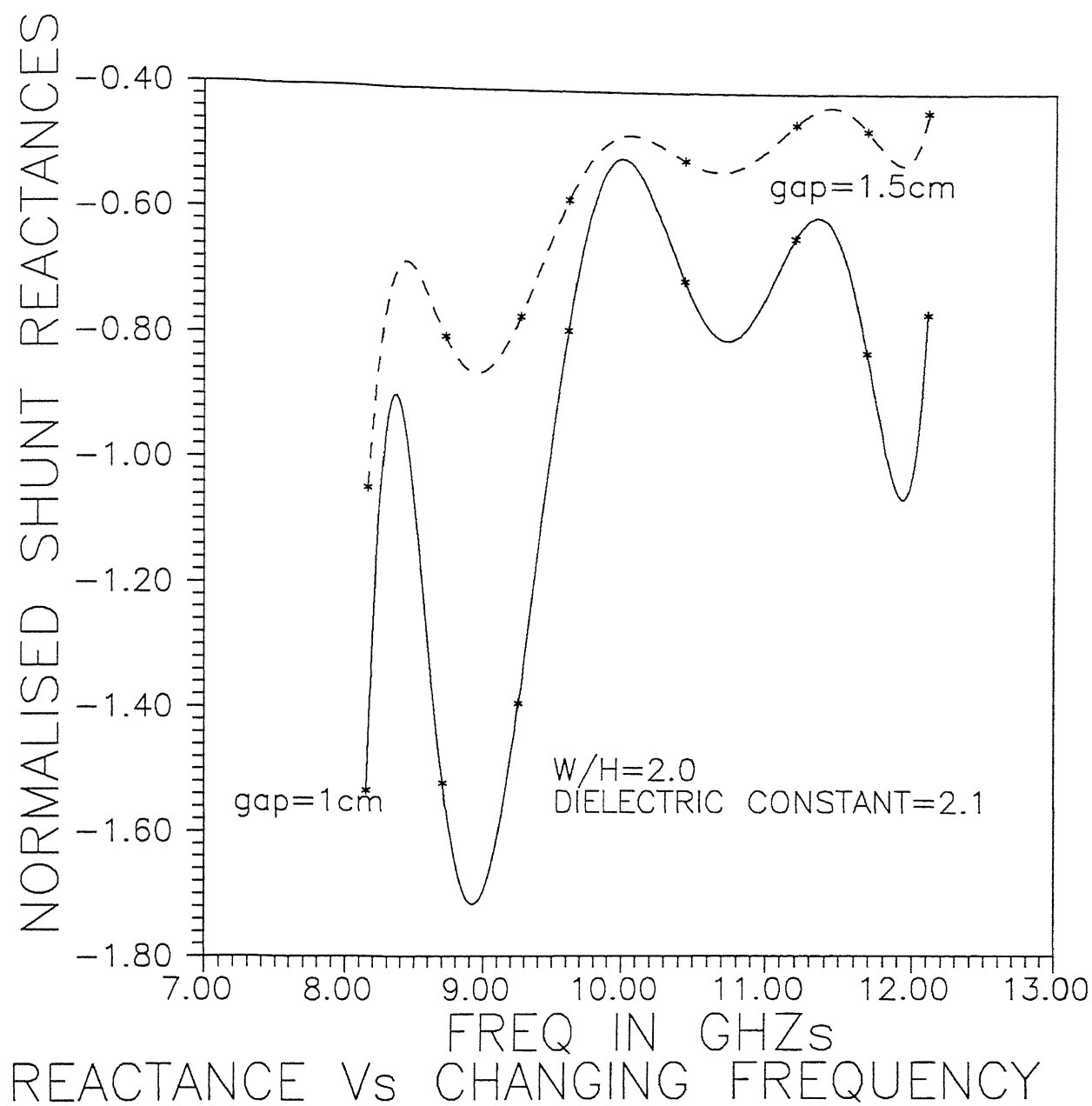


Figure 4-13

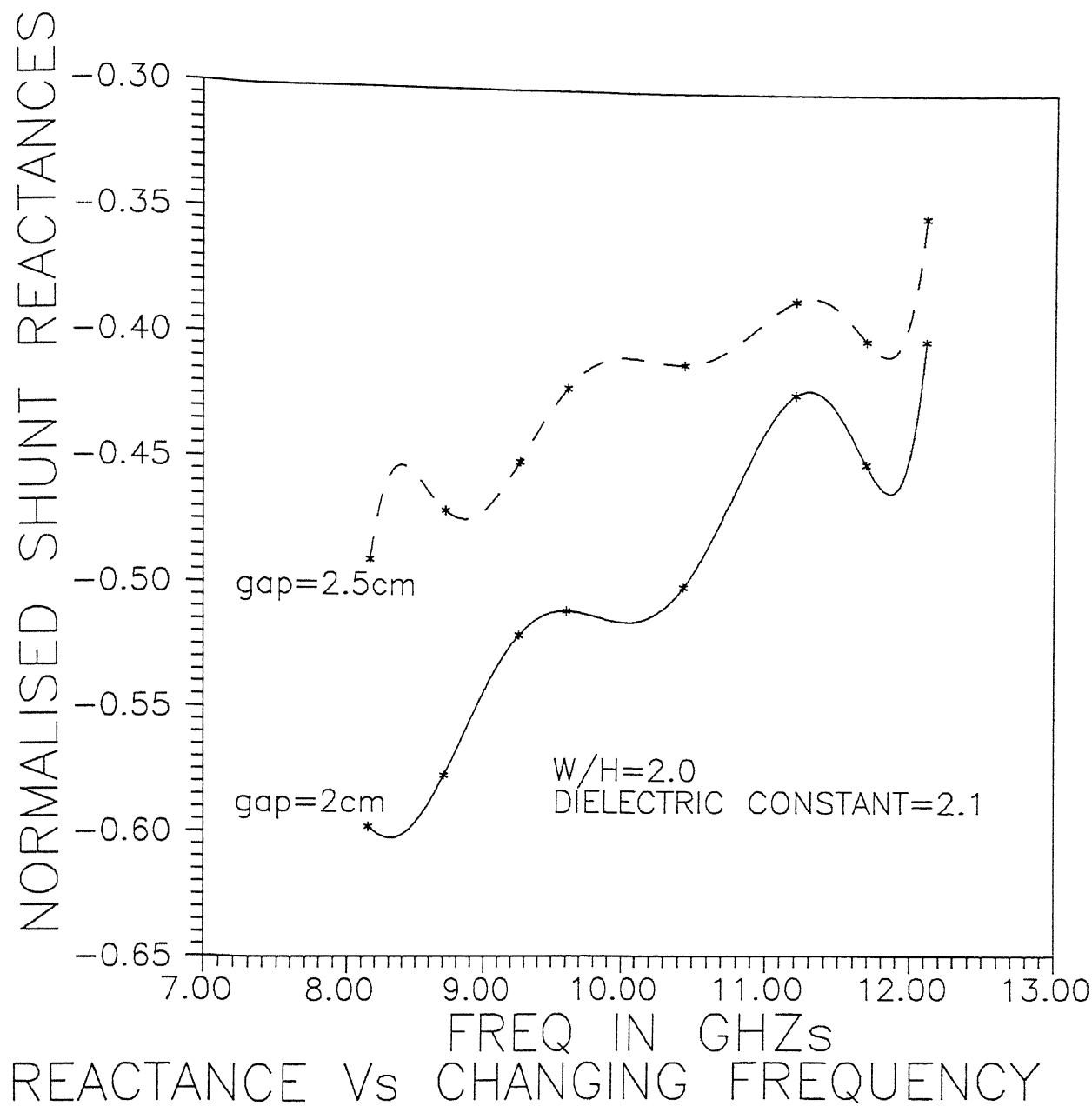


Figure 4.14

Chapter 5

REALISATION OF A BAND PASS FILTER USING AIR GAP DISCONTINUITY IN IMAGE LINE

Using the air gap discontinuity reactance parameters of its T-network model, a band pass filter was realised. The design methodology of the filter was as per conventional microwave filter design.

5.1 SPECIFICATIONS OF THE FILTER

Following specifications were chosen for the filter design:-

- Central frequency = 8.146 GHz
- Passband = from $f_1 = 7.746$ GHz to $f_2 = 8.546$ GHz
- Bandwidth = 800 MHz (10 %)
- Chebyshev 0.5 dB ripple
- Attenuation of minimum 10 dB at $f_a = 7$ GHz and at $f_b = 9.3$ GHz

From guide wavelength λ_g Vs frequency curve (fig 5.1), we find out different values of λ_g at frequencies f_1, f_2, f_a and f_b , which are given below:-

$$f_1 = 7.746 \text{ GHz}; \quad \lambda'_1 = 40.1 \text{ mm} \quad (5.1)$$

$$f_2 = 8.546GHz; \quad \lambda'_2 = 30.9mm \quad (5.2)$$

$$f_a = 7.000GHz; \quad \lambda'_a = 44.8mm \quad (5.3)$$

$$f_b = 9.300GHz; \quad \lambda'_b = 27.86mm \quad (5.4)$$

mean central frequency

$$f_o = \sqrt{f_1 f_2} = \sqrt{7.746 * 8.546} = 8.136GHz \quad (5.5)$$

mean guide wavelength

$$\lambda'_o = \frac{\lambda'_1 + \lambda'_2}{2} = \frac{40.1 + 30.9}{2} = 35.5mm \quad (5.6)$$

fractional bandwidth in terms of frequency

$$w_f = \frac{f_2 - f_1}{f_o} = 0.8/8.136 = 0.0983\% \quad (5.7)$$

fractional bandwidth in terms of guide wavelength

$$w_\lambda = \frac{\lambda'_1 - \lambda'_2}{\lambda'_o} = \frac{40.1 - 30.9}{35.5} = 0.26 \quad (5.8)$$

The normalised frequency mapping from low pass to band pass filter is as follows:-

$$(\omega'/\omega'_1)at f_a = 2/w_\lambda \left[\frac{\lambda'_o - \lambda'_a}{\lambda'_o} \right] = 2/0.26 \left[\frac{35.5 - 44.8}{35.5} \right] = -2.0151 \quad (5.9)$$

and,

$$(\omega'/\omega'_1)at f_b = 2/w_\lambda \left[\frac{\lambda'_o - \lambda'_b}{\lambda'_o} \right] = 2/0.26 \left[\frac{35.5 - 27.86}{35.5} \right] = 1.655 \quad (5.10)$$

For finding out the number of elements we consider equation 5.10, since restrictions on lower value of ω'/ω'_1 decides the number of elements. Referring to Matthai & Jones [20] fig 4-03-7, we get for the value in equation 5.10, number of elements $n=3$.

Now, from the same fig 4-03-7 of [20], we see that, at $f_a = 7$ Ghz, attenuation $L_a = 20$ dB and, at $f_b = 9.3$ Ghz, attenuation $L_a = 15$ dB

Since requirement stipulated in the specifications asked about 10 dB attenuation at above two frequencies, the specification requirements have been adequately met.

The prototype values of elements, which are obtained from table 4-05-2 of [20] are as follows:-

$$g_0 = 1.0$$

ser. no.	discontinuity width 2s(mm)	K	$\phi(\text{radian})$
1	3	0.6934	1.425
2	4	0.6865	1.422
3	5	0.64847	1.413
4	6	0.62	1.39
5	7	0.5872	1.372
6	8	0.55	1.34
7	9	0.53	1.33
8	10	0.4596	1.3233
9	15	0.4082	0.5898

Table 5.1: VARIATION OF K AND ϕ WITH DISCONTINUITY WIDTH

$$g_1 = 1.5963$$

$$g_2 = 1.0967$$

$$g_3 = 1.5963$$

$$g_4 = 1.0$$

$$g_5 = 1.0$$

The inverter parameters are as follows:-

$$K_{01}/Z_0 = K_{34}/Z_0 = \sqrt{\pi w_\lambda / 2g_0g_1w'_1} = \sqrt{\pi * 0.26/2 * 1 * 1.5963 * 1} = 0.5058 \quad (5.11)$$

$$K_{23}/Z_0 = K_{12}/Z_0 = \pi w_\lambda / 2w'_1 * 1/\sqrt{g_1g_2} = \pi * 0.26/2[1/\sqrt{(1.5963)(1.0967)}] = 0.31 \quad (5.12)$$

From the values of $\overline{X_{se}}$ and $\overline{X_{sh}}$, K and ϕ can be calculated by using following two equations[20]:-

$$\phi = -\tan^{-1}(2\overline{X_{sh}} + \overline{X_{se}}) - \tan^{-1}\overline{X_{se}} \quad (5.13)$$

and,

$$K = \tan(\phi/2 + \tan^{-1}\overline{X_{se}}) \quad (5.14)$$

A tabular representation of K and ϕ values for an air gap dscontinuity width from 3mm to 15 mm is given in table 5.1.A plot of the same data appaears in fig 5.2 and in fig 5.3..From these plots we find out required gap length for specified filter design and then note down corresponding value of ϕ .

From fig 5.2 and 5.3, we find out the value of discontinuity air gap length ($2s$) corresponding to K as obtained in equation 5.11 and 5.12. Simultaneously, we note down the value of ϕ for that value of $2s$. Accordingly, we have,

$$\text{For, } K_{01}/Z_0 = K_{34}/Z_0 = 0.51; 2s_1 = 2s_4 = 8.5\text{mm}; \phi_{01} = \phi_{34} = 1.325\text{radians} \quad (5.15)$$

and,

$$\text{For, } K_{12}/Z_0 = K_{23}/Z_0 = 0.31, 2s_2 = 2s_3 = 20\text{mm}; \phi_{12} = \phi_{23} = 0.06\text{radians} \quad (5.16)$$

For finding out length of resonators, ϕ has to be deducted from $\lambda/2 = \pi$. Hence, we have,

$$\theta_1 = \pi - (\phi_{01} + \phi_{12})/2 = 1.57\text{radians} \quad (5.17)$$

$$\theta_2 = \pi - (\phi_{12} + \phi_{23})/2 = 3.04\text{radians} \quad (5.18)$$

Thus, we have, resonant lengths

$$l_1 = l_3 = \frac{\theta_1 \lambda_0'}{2\pi} = 8.85\text{mm} \quad (5.19)$$

$$l_2 = \frac{\theta_2 \lambda_0'}{2\pi} = 17.40\text{mm} \quad (5.20)$$

A diagrammatical representation of complete filter design along with length of input and output section lengths appear in fig 5.4. A plot of filter S_{21} parameter against frequency appears in fig 5.5.

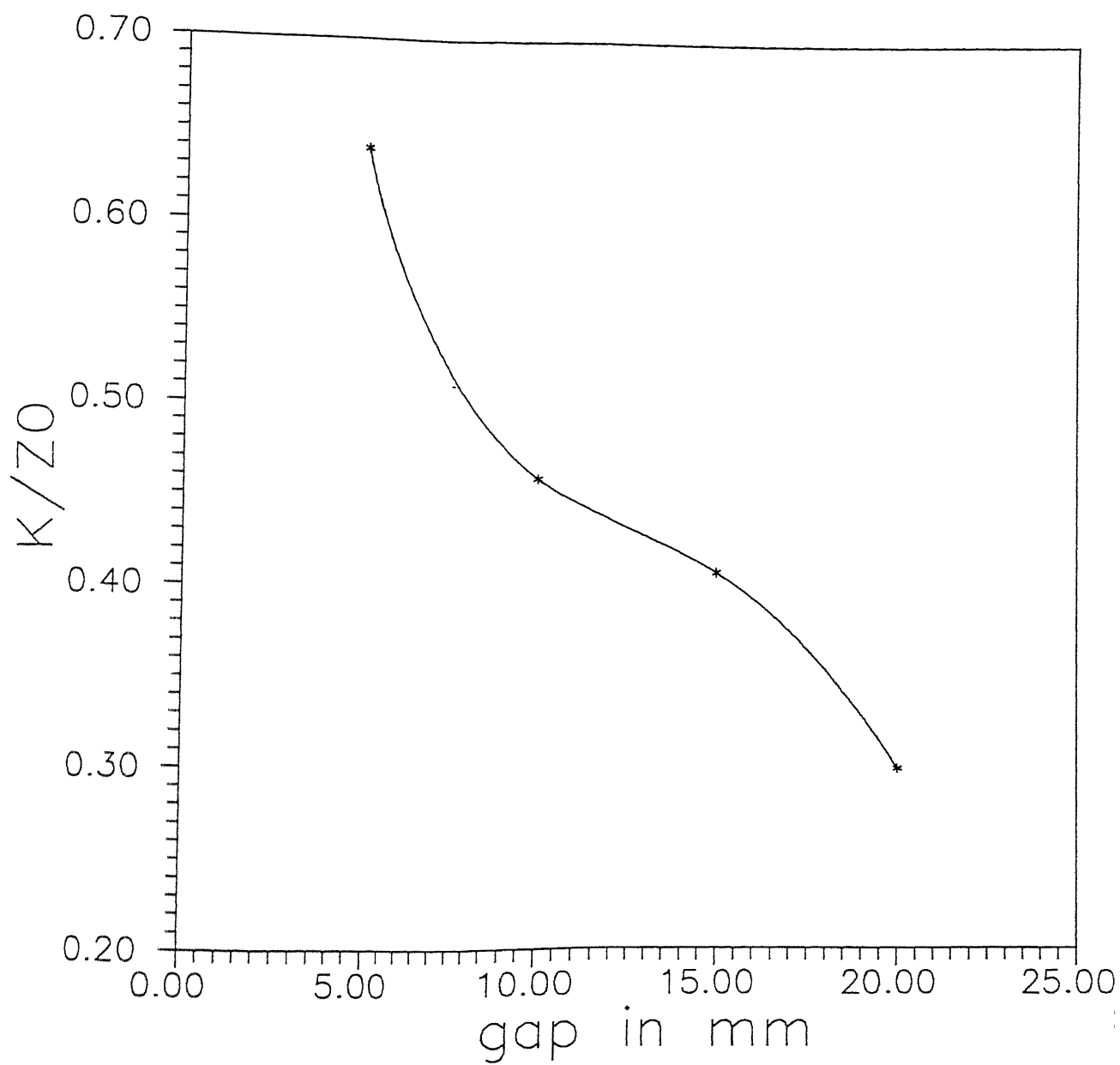


Figure 5.2

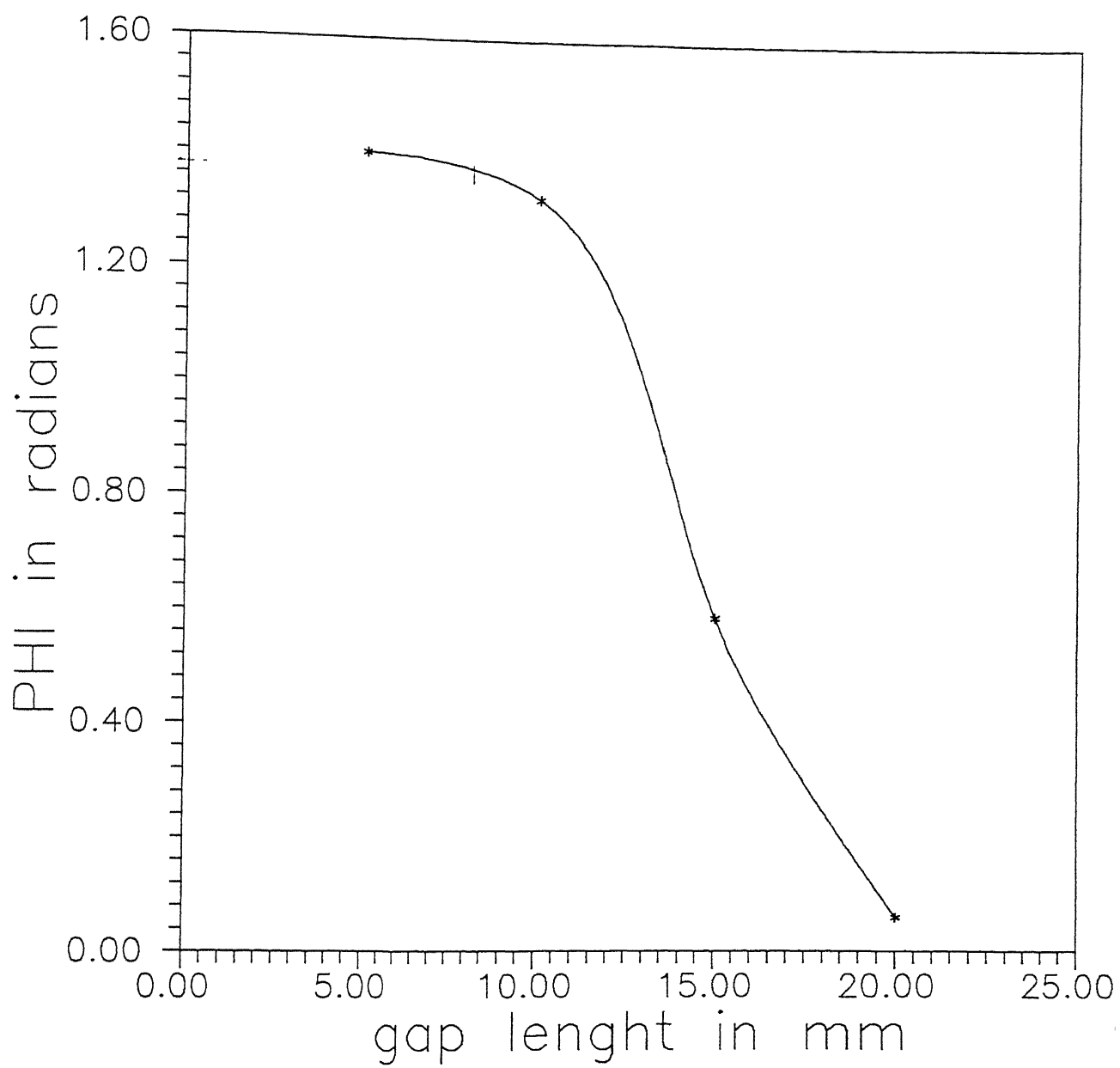


Figure 5.3

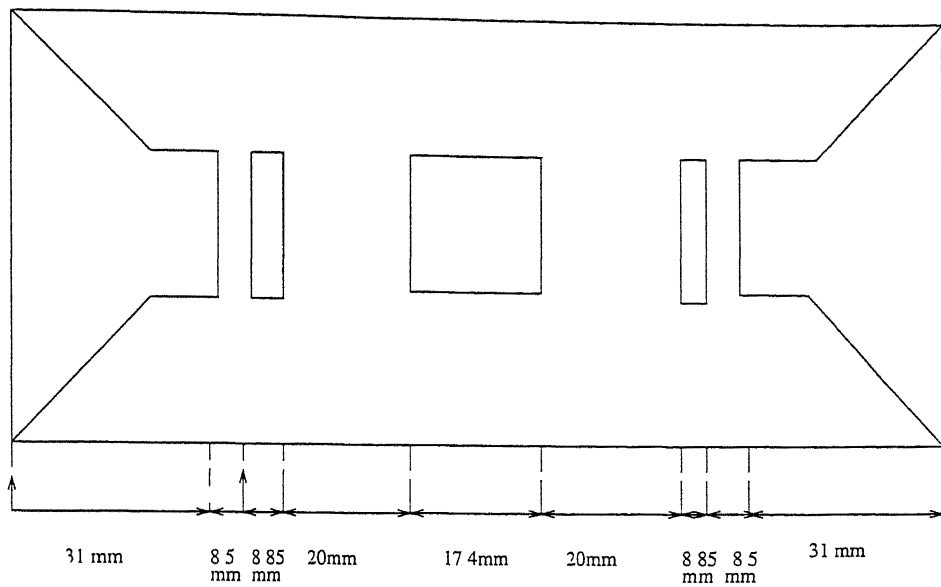


Figure 5.4: A SCHEMATIC DIAGRAM OF BAND PASS FILTER

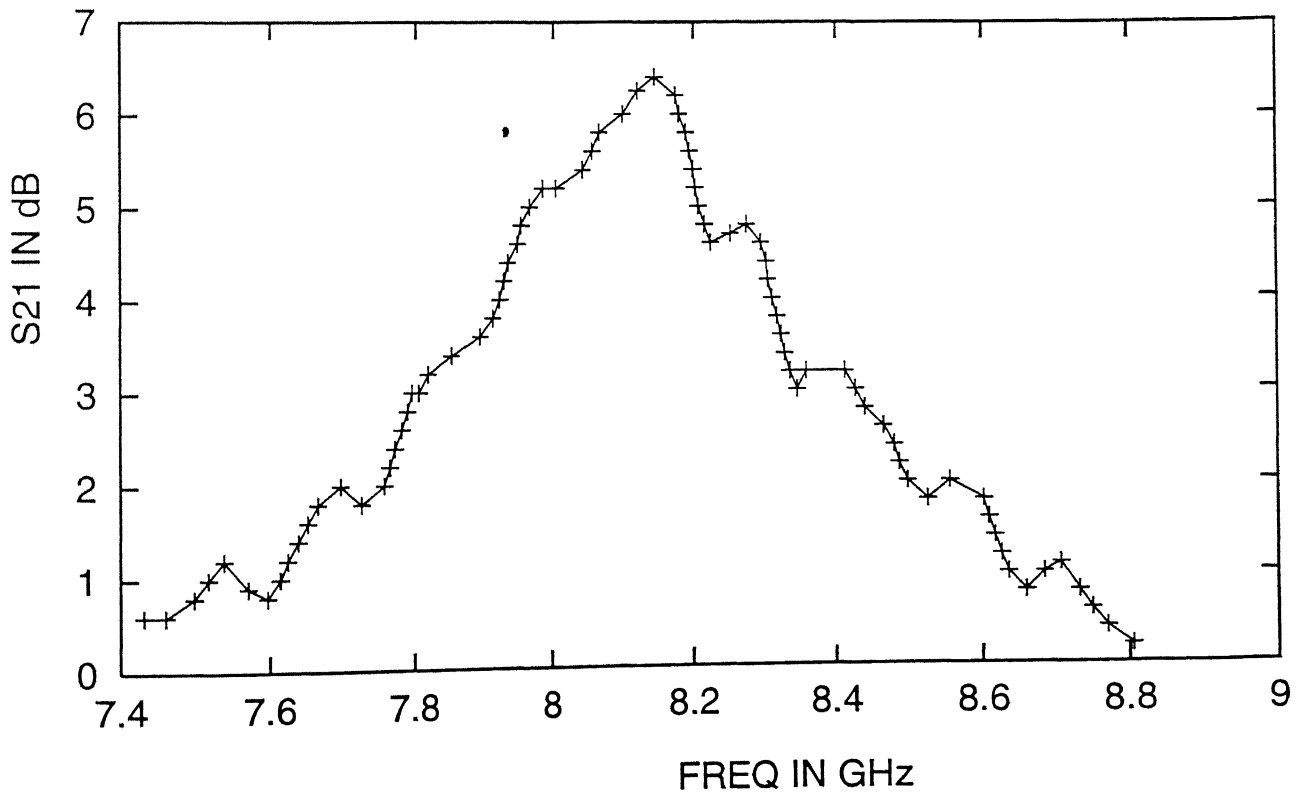


Figure 5.5: TRANSMISSION COEFFICIENT S21 Vs FREQUENCY(GHz) FOR BAND PASS FILTER

Chapter 6

CONCLUSION

Work presented in this thesis basically comprised of the following aspects:-

- Characterisation of air gap type of discontinuity in an image line.
- Characterisation of notch type of discontinuity in an image line.
- Realisation of band pass filter based on air gap discontinuity data.

From the analysis of results obtained, following deductions can be drawn:-

- Transverse resonance technique can be used for analysis of any symmetrical discontinuity in a lossless line.
- Enclosing a image line inside a metallic waveguide type of housing increases the dispersion and ,thus, affects the lower cut-off frequency.
- A filter design based on such a discontinuity model reactance parameters gives fairly accurate results.

The band pass filter designed gave fairly accurate experimental results. However, following improvements can be incorporated in the experimental mechanism:-

- A more stable and accurate oscillator, other than Wavetek model used, can be employed as a source of energy.
- Scattering parameters can be more accurately obtained on Network Analyser HP8510C using TRL calibration techniques.
- Method of launching energy can be undertaken after detailed theoretical investigation of radiations from tapered edges of dielectric lines.

- A coaxial probe to measure fields on the image line, as designed by Solbach[15] can be fabricated and measurements undertaken thereafter.

6.1 RECOMMENDATIONS

Following recommendations are suggested to be undertaken as a sequel of present work:-

- A detailed theoretical investigation of image line discontinuity in both open and shielded environment should be done.
- Experimental measurements should also be performed with other mode launchers viz. a slot in the ground plane, Yagi-Uda array, horn launchers etc.
- Image line experimental analysis can be frequency scaled by changing the dimensions of the dielectric line[9]. The same experimental work can be repeated for millimetric wave region by suitably selecting the line dimensions.

References

- [1] E.A.J Marcatili, "Dielectric rectangular waveguide and directional coupler for integrated optics", *Bell System Technical Journal*, vol. 48, september 1969, pp 2079-2102.
- [2] J.E. Goel, " A circular harmonic computer analysis of rectangular dielectric waveguides", *Bell System Technical Journal*, vol.48, september 1969, pp 2133-2160.
- [3] Klaus Solbach and Ingo Wolff, "The Electromagnetic Fields and the Phase Constants of Dielectric Image Lines", *IEEE Trns.on Microwave Theory and Technique*, vol.MTT-26, April 1978, pp 266-274.
- [4] Tatsuo Itoh and R.Sorrentino, "Transverse resonance analysis of finline discontinuities," *IEEE Trans.on Microwave Theory and Technique*, vol. MTT-32, 1983, pp. 1633-1638
- [5] Animesh Biswas, "Studies on finline discontinuities and their application in periodic structures and filters," P.hd. Thesis, Indian Institute of Technology, New Delhi, 1988
- [6] Lalat K Pradhan, "Full Wave Analysis of Single and Coupled Shielded Image Guide for Millimetric Wave Applications" , M.Tech.Thesis, Indian Institute of Technology, Kanpur, May 1994
- [7] E.Pic and W.J.R.Hoefer, "Experimental characterisation of finline discontinuities using resonant technique," *IEEE MTTS int.Microwave symp,Digest*, 1981, pp.108-110
- [8] Klaus Solbach, "The fabrication of dielectric image lines using casting resins and properties of the lines in the millimetric wave range", *IEEE Trans. on Microwave Theory and Technique*, Vol.MTT-24, November 1976, pp.879-887.

- [9] Richard. J. Collier and Robin D. Birch, "The bandwidth of image guide", *IEEE Trans.on Microwave Theory and Technique*, vol.MTT-28, August 1980, pp 932-935
- [10]] Klaus Solbach, "The measurement of the radiation losses in the dielectric image line bends and the calculation of a minimum acceptable curvature radius", *IEEE Trans. on Microwave Theory and Technique*, Vol.MTT-27, January 1979, pp.51-53.
- [11] D D King, "Properties of dielectric image lines," *IRE Trans. Microwave Theory and Technique.*, vol.MTT-3, March 1955, pp 75-81.
- [12] D D King and S.P Schlesinger, "Losses in dielectric image lines," *IRE Trans.Microwave Theory and Technique*, vol.MTT-5, January 1957, pp 31-35.
- [13] ———, "Dielectric image lines," *IRE Trans.Microwave Theory and Technique*, vol.MTT-6, July 1958, pp. 291-299.
- [14] Tatsuo Itoh, "Inverted strip dielectric waveguide for millimetric wave integrated circuits," *IEEE Trans. on Microwave Theory and Technique*, Vol.MTT-24, November 1976, pp.821-827.
- [15] Klaus Solbach, "Electric probe measurements on dielectric image lines in the frequency range of 26-90 GHz," *IEEE Trans.on Microwave Theory and Technique*, vol.MTT-26, October 1978, pp.755-758.
- [16] Klaus Solbach, "Slots in dielectric image lines as mode launchers and circuit elements," *IEEE Trans.on Microwave Theory and Technique*, vol.MTT-29, January 1981, pp.10-16.
- [17] R.M.Knox, "Dielectric waveguide:A low cost option for ICs," *IEEE Trans.on Microwave Theory and Technique*, vol.MTT-15, March 1976, pp 56-67.
- [18] W.K.McRitchie and J.C.Beal, "Yagi-Uda array as a surface-wave launcher for dielectric image lines," *IEEE Trans.on Microwave Theory and Technique*, vol.MTT-20, August 1972, pp.493-496.
- [19] H.Jacobs, et al., "Measurement of guide wavelength in rectangular dielectric waveguides," *IEEE Trans.on Microwave Theory and Technique*, vol.MTT-24, November 1976, pp.815-820.